

Wind Actions on Flat-Roof-Mounted Photovoltaic Panels

A Comparison of Design Guidelines

Jonas Westin

Avdelningen för Konstruktionsteknik
Lunds Tekniska Högskola
Lunds Universitet, 2011

Avdelningen för Konstruktionsteknik

Lunds Tekniska Högskola
Box 118
221 00 LUND

Department of Structural Engineering

Lund Institute of Technology
Box 118
S-221 00 LUND
Sweden

Wind Actions on Flat-Roof-Mounted Photovoltaic Panels

Vindlaster på solpaneler monterade på platta tak

Jonas Westin

2011

Rapport TVBK-5195

ISSN 0349-4969

ISRN: LUTVDG/TVBK-11/5195+88p

Master's Thesis

Supervisors: M.Sc. Stephan Hippel, Prof. Annika Mårtensson

January 2011

Abstract

Wind actions on roof-mounted solar collectors differ from those on an open range-deployment, due to turbulence and wind stream deflection induced by the underlying building. As of December 2010, no construction codes in effect describes the wind loads on such structures, with the exception of the preliminary standard *NVN 7250* from the Netherlands, with the latest draft released in 2007.

The roofs considered for this type of plants often consists of large-surface flat-roofed industrial halls with tar-bitumen roof sheeting. Penetrating the roofing for fixtures of the solar collectors is often not allowable, so instead, wind-induced uplift forces are counter-acted by attaching ballast to the photovoltaic mounting systems. This practice causes the need for both safe and economical wind action guidelines, since uneconomical dimensioning causes the ballast quantities to exceed the residual load capacity of the roof, rendering the construction infeasible.

A static model was developed for a typical photovoltaic mounting system. Results from three wind tunnel investigations on roof-mounted photovoltaics for different roof geometries were gathered, and the guidelines from the Dutch pre-standard NVN 7250 were adapted to the geometric boundary conditions of the respective studies. For all approaches to the wind loads, roofs are divided into different load areas, where modules situated in the different load areas are assigned different wind loading coefficients. The static model was used to determine the ballast quantities needed for static equilibrium, using the results from the wind tunnel investigations, and the adaptations from the NVN 7250 respectively.

The pre-standard was found to underestimate the ballast compared to one of the wind tunnel investigations, while significantly overestimating the ballast compared to the two other results. Further, large differences were found between the wind loading coefficients from the wind tunnel investigations, derived for seemingly similar module layouts and mounting system geometries. This led to the conclusion that the aerodynamic properties of the mounting system itself plays a large role in determining the wind loads. The description of the mounting systems in the pre-standard, where the systems from the investigations all fall into the same category, seems insufficiently fine-grained, since the wind actions in the end turned out both over- and underestimated. It is therefore not advisable to use the pre-standard NVN 7250 to dimension mounting systems and verifying static equilibrium.

Preface

This study was carried out with the kind sponsorship of PUK-Werke KG, Berlin, between May and November 2010. It was conducted in preparation for the expansion of a dimensioning software for photovoltaic mounting systems that was previously written by the author. The expansion concerns the dimensioning of mounting systems for photovoltaic collectors on flat roofs, for which the wind actions proved to be a complex subject.

I would like to thank my supervisors, Stephan Hippel at PUK-Werke KG and Prof. Annika Mårtensson at the Division of Structural Engineering of LTH, for their invaluable assistance. Further, I would like to thank Prof. Chris Geurts at TU Eindhoven, Prof. Hans Ruscheweyh at Ruscheweyh Consult GmbH, and Rolf-Dieter Lieb of IFI Institut für Industriaerodynamik GmbH for sharing articles and results and for answering questions. Without their assistance, this study would not have been possible.

Finally, I would like to thank my friends and family for their encouragement.

Berlin, December 2010

Jonas Westin

Contents

1. Introduction	1
1.1. Aim and purpose	2
1.2. Scope and limitations	3
1.3. Method	3
2. Review of products and research	5
2.1. Existing Products	5
2.1.1. Frames of aluminium or sheet metal profiles	5
2.1.2. Frames of aluminium or sheet metal profiles, connected laterally	6
2.1.3. Load-bearing sheet metal plates / frames with wind protection	7
2.1.4. Gravel-filled troughs	7
2.1.5. Fastening methods	8
2.1.6. Summary: Geometrical boundary conditions	8
2.2. Theory of wind loads	9
2.2.1. Analysis of wind	9
2.2.2. Determining wind pressure coefficients	10
2.3. Wind load investigation	13
2.3.1. Current construction standards	14
2.3.2. Previous investigations of wind loads	14
2.3.3. Summary with respect to geometrical parameters	16
2.3.4. Conclusions from previous research	19
3. Loads and statics	23
3.1. Description of structure	23
3.1.1. Actions on structure	24
3.2. Section forces	26
3.2.1. Longitudinal beam	26
3.2.2. Triangular Substructure	33
4. Wind actions for varying geometries	39
4.1. Standard case according to the NVN 7250	39
4.1.1. Building and mounting system geometry of the base case	39
4.1.2. Wind action model of the NVN 7250	41
4.1.3. Ballast quantity derivation according to NVN 7250	41
4.1.4. Usage example	44
4.1.5. Adaption for real-world usage	48

4.2.	Modules oblique to building walls	49
4.2.1.	Building and mounting system geometry	50
4.2.2.	Wind action model according to Ruscheweyh and Windhövel	51
4.2.3.	Ballast quantity derivation according to Ruscheweyh and Windhövel	52
4.2.4.	Application - Ruscheweyh and Windhövel	56
4.2.5.	Adaption of geometry to NVN 7250	57
4.2.6.	Comparison	58
4.3.	Varying roof height	61
4.3.1.	Building and mounting system geometry	61
4.3.2.	Wind actions	61
4.3.3.	Ballast	63
4.3.4.	Application of results from case study	63
4.3.5.	Adaption of roof geometry to NVN 7250	65
4.3.6.	Comparison	67
4.4.	Standard case, comparison with wind tunnel results	70
4.4.1.	Building and mounting system geometry	70
4.4.2.	Actions	71
4.4.3.	Ballast determination	71
4.4.4.	Application of NVN 7250	71
4.4.5.	Comparison	71
4.5.	Results and tendencies from the comparisons	72
5.	Conclusion	73
5.1.	Outlook of creating reusable design guidelines	73
5.2.	Critical review of work presented	74
5.3.	Recommendations for future work at PUK-Werke KG	74
A.	Excerpts from NVN 7250	79
A.1.	Appendix A.7: Height differences on roofs	79
A.2.	Appendix A.8: Roof lanterns and penetrations	80

1. Introduction

The amount of solar energy produced in Germany has seen an unprecedented increase in the last two decades. In an effort to support this, the Renewable Energy Sources Act (*Erneuerbare-Energie-Gesetz*, Bundesgesetzblatt I S. 305) was passed by the German Bundestag in the year 2000, with the aim to double the share of renewable energy in the German power production until 2010. As a part of this objective, additional efforts were put into introducing photovoltaic energy production in the national power grid (Bundesministerium für Umwelt, Naturschutz und Reaktorsicherheit, 2010). A guaranteed price for energy produced by solar power was introduced, and further subsidies for each kWh fed into the power grid was guaranteed for 20 years after starting to produce power (Bundesministerium für Umwelt, Naturschutz und Reaktorsicherheit, 2010).

From 2000 to 2008, the energy contribution from photovoltaic power in Germany grew from 64 GWh to over 4,000 GWh, and the yearly installed output grew from 42 to 1,500 MW Peak (Bundesministerium für Umwelt, Naturschutz und Reaktorsicherheit, 2009). During this time, the total contribution from renewable energy sources also grew from 6.3% to 15.1%. Further, the amount of solar panels produced in Germany grew from 16 MW Peak in the year 2000 to 1,838 MW Peak in 2008 (Bundesverband Solarwirtschaft, 2010b), and the number of people employed in solar energy from 11,000 in 2000 to 78,000 in 2008 (Bundesverband Solarwirtschaft, 2010a). From 2000 to 2008, the cost per installed kW also sank from circa €6,000 to €3,135, partially thanks to increased production, but also thanks to increased efficiency of both the panels and of peripheral components, such as power inverters (Janzig, 2010).

During this development, the desire arose among property owners to use the flat roofs of larger industrial halls for photovoltaic energy production. Flat industrial roofs provide the possibility of freely orientating the panels according to sun angles (Weller et al., 2009). The solar collectors are typically mounted at an angle of 30 degrees, with a light steel structure to keep them in position. However, the exposed positioning of the panels and turbulence caused by building geometry, causes roof-mounted panels to experience large uplift forces from the wind (Weller et al., 2009). For constructional and service expectancy reasons, it is often undesirable to penetrate the roofing with a mechanical fastening, and instead, additional ballast is attached to the mounting system (Erfurth, 2001). One traditional approach for smaller roof installations has been to assume the highest wind load coefficients found in the wind action guidelines (Geurts and van Bentum, 2007, p. 208), a clearly uneconomical approach. The limited residual load capacity of industrial roofs, combined with the use of ballast instead of penetrative fastenings, makes economical wind load coefficients desirable and often necessary (Ruscheweyh and Windhövel, 2005). On the other hand, this must not reduce the safety of the approach. So far, many manufacturers of mounting systems have been conducting project-specific wind tunnel investigations to

1. Introduction

become better wind load data, which is only economical for very large projects.

The limited residual load capacity of common industrial roof structures, thus limits the wind load assumptions for designing these systems at the upper bound, making an economical approach desirable (Ruscheweyh and Windhövel, 2005). Of course, this doesn't void the need for safety in the load assumptions.

The influence on the wind from the underlying building induces more complex and varying wind actions on the panels, compared to open range solar plants. The need for safe dimensioning guidelines on one hand, and economical dimensioning on the other, has led engineers to conduct elaborate investigations early in the design process. This is however becoming less and less practical in a growing market where solar power investors make inquiries to multiple manufacturers, and where manufacturers wish to process offers quicker to accommodate the increasing demand. It is in this case desirable to have more widely applicable wind load assumptions for the roof-mounted panels.

As a previous project, realized during fall 2009 – spring 2010, the author developed a dimensioning software for the open range photovoltaic mounting systems manufactured by PUK-Werke KG in Berlin. Through this software, optimal dimensions and bearing distances are derived to produce the most inexpensive mounting system for the given geometrical and geographical input. This optimization, impossible with a manual dimensioning due to the tediousness of the calculations, has made PUK-Werke KG's mounting system product line more competitive. The desire is now to create a similar software for mounting systems aimed at industrial roofs, and the aim of this study is to lay the theoretical foundation for the upcoming project, especially with regards to wind loads.

1.1. Aim and purpose

The purpose of the study presented here is to suggest and investigate the plausibility of a method for assessing the wind actions on flat-roof-mounted solar collectors and the ballast quantities needed to resist the uplift forces when penetrating the roofing is not permissible.

Existing products for the purpose of mounting solar panels to flat roofs are surveyed in order to determine the variations in geometry of such a structure. Further, existing research on the subject of wind loads is investigated and summarized. From this, the load distribution and spatial variation, that the static model must accept, can be determined. It is also concluded for which situations usable wind load assessments exist, and for which cases an approach needs to be developed. The methods used for determining wind load coefficients in the design guides found and used in this document are reviewed, to give some technical background.

A static model of the mounting systems is developed with consideration to the geometrical boundaries and load assumptions previously identified. Relevant loads and load combinations are also assembled, both for dimensioning the mounting system and for determining the added weight to prevent displacement. Since the model is to be computerized, the description focuses on systematizing and dividing load cases and components rather than finding dimensioning heterodynes and maximum stress positions on structural members.

Situations where the current state of research provide design guidelines are identified, and the process of deriving the wind loads is shown. A concrete example is shown, for which wind loads, necessary added weight, and resulting forces acting on the building are calculated.

Results from wind tunnel investigations are gathered, and adaptations of the existing wind action guidelines to the specific boundary conditions of the investigations are suggested. Wind loads and resulting actions on the building are determined and compared between the suggested approaches and their respective case studies, with respect to safety and economy. For each situation, it is determined if the approach is usable or not.

Finally, the suggested approaches to determine wind actions are evaluated with regards to their applicability and economy. A critical review is done regarding the simplifications of the model and considerations needed when applying it, and recommendations for proceeding with the development of a wind action model are presented.

1.2. Scope and limitations

The investigation here covers solar collectors mounted on large-surface roofs with a roof pitch small enough to be neglected (defined in the EN-1991-1-4 as roofs with a slope of less than 5 degrees). The mounting systems of interest yields a module pitch between 15 and 30 degrees relative to the roof surface. The actions on structures taken into consideration are limited to those described in the Eurocode EN 1991:1-3 (snow loads) and EN 1991:1-4 (wind) into consideration. No national exceptions and additions are examined. Further, only the large structural elements are considered in the dimensioning; connection details and final implementation of the structure are being left out. These parts are left out since the focus here lies on wind actions rather than constructive details. Just as in the wind action descriptions in the existing codes, limiting the scope to simpler geometries makes prediction and parameterization of the wind actions possible in the first place.

1.3. Method

In the first part of this thesis, examination of products and existing wind research on wind loads on roof-mounted solar panels, is conducted as a literature study. Boundary conditions for the continued work are determined regarding structure geometry and load geometry. A basic approach for determining wind loads is suggested using the results from this study, and non-standard building geometries are identified, for which approaches to determine the wind loads are suggested using the existing results.

A static model of the roof-mounted solar panels is developed using Bernoulli-Euler beam theory and the flexibility method for statically indeterminate systems as described by Meskouris and Hake (1999). This model is implemented in a computer program to handle the vast amount of calculations needed for the comparisons of approaches to determining the wind loads.

The computer program is used to determine wind loads acting on modules and necessary ballast for the examined buildings and module configurations. Existing wind load

1. Introduction

certificates or specific wind tunnels studies have been obtained for the non-standard geometries, and the for each case specific boundary conditions are entered into the program. Wind loads and ballast are determined using the wind load coefficients given in the case studies and by the approaches suggested in this report. The results are compared for the specific outcomes, especially with respect to situations where the suggested approaches to determine the wind loads underestimates the wind action compared to the case studies.

2. Review of products and research

A vast array of mounting system products exists on the current market. On the other hand, few studies regarding the aerodynamic properties of these structures have been published. Both areas are reviewed in this section to determine the variations of geometry and wind action models which the static model later developed needs to take into account.

2.1. Existing Products

Below follows a short overview of existing mounting systems on the market, as of December 2010. The list of products and manufacturers is not intended to be exhaustive. Mounting systems for solar panels on flat roofs can be divided into four categories. The fastening methods also mentioned in this section are in general applicable to all types of mounting systems mentioned here.

2.1.1. Frames of aluminium or sheet metal profiles

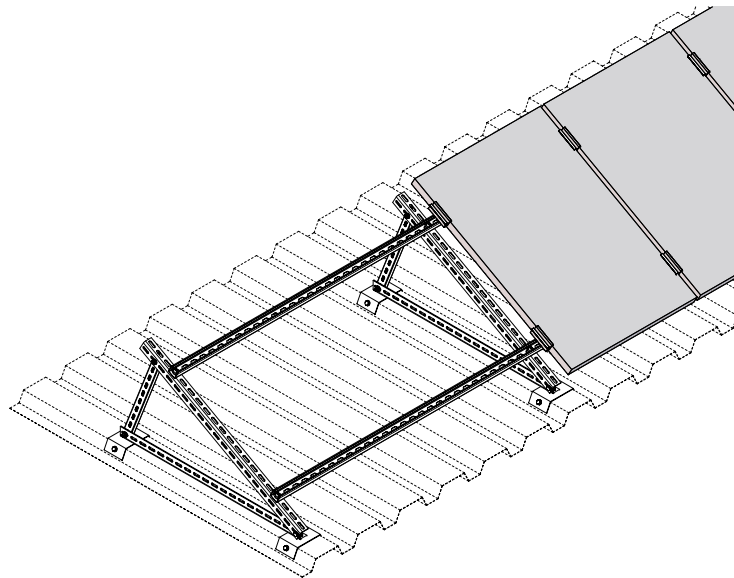


Figure 2.1.: Support structure made out of sheet metal profiles (PUK-Werke KG, 2010)

2. Review of products and research

The first, and most common, product category consists of simple triangles of sheet metal profiles, with longitudinal beams to carry the modules, as shown in Figure 2.1. Among the manufactureres are PUK-Werke KG, Schletter GmbH (CompactGrid series), and Altec Solartechnik (AlFach) (PUK-Werke KG (2010), Schletter GmbH (2010a) and Altec Mittig und Manger GmbH (2010) respectively). The frames are made of either sheet metal or aluminium profiles. The frames are often joined in rows as long as the roof layout permits.

Many of these systems —similar to the ones mentioned below— can be attached to ballast to neutralize uplift forces and prevent horizontal displacement through friction between the supports and the roof surface. This can be achieved with gravel-filled troughs or with concrete slabs. Some systems are even designed to be loaded with pre-cast slabs made for gardening use (Altec Mittig und Manger GmbH, 2010). An advantage with gravel troughs (on gravel roofs) is that the existing gravel can be used for ballast, which decreases the net additional weight being brought onto the roof (though, with concrete elements, the gravel layer still has to be partially removed).

2.1.2. Frames of aluminium or sheet metal profiles, connected laterally

A product similar to those in Section 2.1.1 are the triangular racks, with rails connecting the rows to one another. Examples are the MS-Connect PC2 series from Sun-Value GmbH (2010b) (as seen in Figure 2.2), the SOL-50 series from Solare Energiesysteme Nord Vertriebsgesellschaft mbH (2010), and the CompactVario series from Schletter GmbH (2010b). Some manufacturers claim that this helps neutralizing transient peak uplift forces by making it less probable that peak loads coincide on the entire structure as the load surface is increased (Schletter GmbH, 2010c).



Figure 2.2.: Laterally connected system (Sun-Value GmbH, 2010b)

2.1.3. Load-bearing sheet metal plates / frames with wind protection

In order to minimize the need for loading weight, manufacturers seal their frames with sheet metal or construct the frame completely out of sheet metal, as seen in Figure 2.3. This is supposed to prevent the wind from exerting force on the solar panel from below, and thus creating a lifting force. Instead, since all the surfaces are aligned upwards, the wind supposedly exerts downward pressure from all directions, and in this way the need for ballast is reduced or completely avoided, according to manufacturers (KNUBIX GmbH, 2010). Examples include Sunposet by Kösslinger Energy GmbH (2010), MS-Connect LC3 by Sun-Value GmbH (2010a), and KNUBIX 100 (KNUBIX GmbH, 2010).



Figure 2.3.: Sheet metal structures (KNUBIX GmbH, 2010)

Further, the frames can be connected in lateral direction as in the previous section, which gives the same benefits.

2.1.4. Gravel-filled troughs

This solution consists of a plastic trough to be filled with ballast (normally gravel) and a few mounting details for the solar panel, as shown in Figure 2.4. These supports will usually only carry one panel per mounting through, and the troughs may or may not be connected into longer rows. Brands on the market include Solarsimplex by Conergy AG (2010) and Renusol ConSole (Renusol Solar Mounting Systems, 2010b).

Since the troughs are only manufactured in a few sizes, adapted to known sizes of solar panels, the dimensioning of such a plant only consists of calculating the needed weight to be added. This is done with simple tables provided by the manufacturer, for example those by Renusol Solar Mounting Systems (2010a).

2. Review of products and research

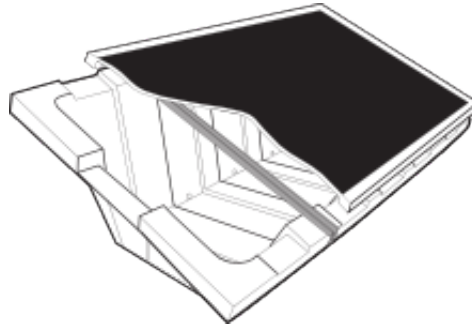


Figure 2.4.: Trough to be filled with gravel (Renusol Solar Mounting Systems, 2010b)

2.1.5. Fastening methods

The fastenings need to be able to equalized wind-induced uplift. There are three methods mainly being used today, depending on the roofing:

1. **Clamps** for trapezoidal sheet metal or clutches for tiled roofs. (Hilti Deutschland GmbH, 2010)
2. Attaching **ballast** to the mounting system, to compensate for uplift forces. The additional weight must also create enough friction to compensate for horizontal support reactions, to prevent displacement (Erfurth, 2001). This is primarily used on bituminous roofing (with or without gravel), where penetrating the roofing is undesirable.
3. Gluing **sleeves of synthetic roofing** sheets onto the underlying roofing, which must be synthetic as well. This method is used by the manufacturer Sunova AG (2010), among others.

Although the fastening method with ballast is the most common, since it doesn't penetrate the roofing and won't cause leaks and decreased service expectancy. Since the ballast is the only thing attaching the mounting system to the roof, the uplift force estimation has to be conservative. A too conservative approach may on the other hand cause the module arrangement to be deemed unfeasible with respect to the load bearing reserve of the roof under consideration.

2.1.6. Summary: Geometrical boundary conditions

The described products all have the triangular substructure in common, be it with one or multiple module rows, and with vertically or horizontally placed modules. The static model developed later will correspond to the mounting systems described in Section 2.1.1 and 2.1.3, since those are the variants most commonly used.

2.2. Theory of wind loads

In this section follows a short introduction to wind loads and building aerodynamics. The methods discussed here apply only to static structures. A static structure is meant as a structure demonstrating only small deflections under wind load (thus not influencing the aerodynamic properties of the structure). The most defining property of a static structure is that the internal action state (stress on structural members) is proportional to the loads acting on the building, and the structural response to changed loads is instantaneous and proportional to the change; that is, no dynamic effects are induced by load variations (Cook, 1990, p. 9).

2.2.1. Analysis of wind

Cook (1985) decomposes wind actions into three parts: *wind climate*, *boundary layer* and *structural influence*. The components all affect the resulting wind actions on a structure, but with different scope and to different extents.

Wind climate

The scope of influence of the wind climate on a location is equivalent to the size of the weather system, roughly 600 km (Cook, 1985, p. 76). This means that all buildings inside this radius are affected by the same wind climate. The variations in wind climate typically have a periodicity of 0.01 cycles/hour ($T = 4$ days), which is the time it typically takes for a weather system to pass and move on.

Boundary layer

The *boundary layer* is the influence from ground friction on the air stream, the reduction of wind speed and increase of turbulence closer to the ground (Cook, 1985, p. 77). The boundary layer typically influences the wind stream up to a height of 2500 m. Typical periods for boundary-layer-induced turbulence are 10 minutes to 3 seconds ($f = 0.001 - 0.3$ Hz).

Structural influence

The smallest turbulence eddies and the fastest pressure variations are induced by the deflection of the wind stream from the building. The building-induced turbulence typically consists of frequencies above 0.3 Hz (Cook, 1985, p. 82)

The influence from the structure on the wind actions comes from the deflection of the air stream from the (bluff) structure geometry (Cook, 1985, p. 167). For example, consider a flat-roofed rectangular building where the wind hits the building normal to one of the faces. The eave of the windward face will deflect the wind flow from the windward regions of the roof, causing what is called a *separation bubble* (see Figure 2.5), that is, a region with negative pressure. If the roof is long enough, the flow then reattaches, causing positive pressure towards the leeward face of the building.

2. Review of products and research

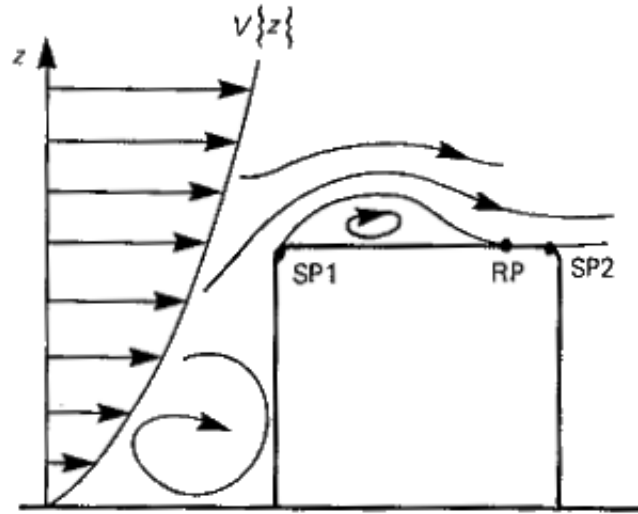


Figure 2.5.: Separation bubble on flat-roofed building (Cook, 1985, p. 172)

Another example of structure-induced influence on the wind action worth mentioning here is the *delta-wing vortex*. The delta-wing vortex occurs when the wind is oblique to the building faces and hits a corner of the flat-roofed building (Cook, 1985, p. 172). This creates large negative pressures in the immediate proximity of the windward corner, but also large uplift forces along the windward eaves of the building. The principle is explained by Figure 2.6.

2.2.2. Determining wind pressure coefficients

The common way to relate the wind actions on a structure to the building geometry is to normalize the actual pressure p on the building surface to the dynamic wind pressure $q(t)$ measured on the chosen reference height z of the building, yielding the *wind loading coefficient* c_p , as shown in Equation (2.1) (Cook, 1990, p. 13).

$$c_p(t) = \frac{p}{q(t)} \quad (2.1)$$

where $q(t)$ is a function of the air density ρ and the wind velocity $V(z)$ on the reference height

$$q(t) = \frac{\rho}{2} V(z)^2 \quad (2.2)$$

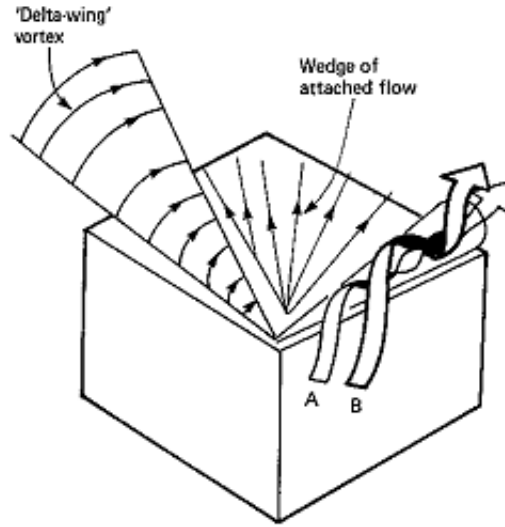


Figure 2.6.: Delta vortices on flat-roofed building (Cook, 1985, p. 173)

The following notations are used in this section:

- \bar{c}_p : Mean pressure coefficient, averaged over time
- c'_p : Root-mean-square, averaged over time
- \hat{c}_p : Maximum peak value
- \check{c}_p : Minimum (largest negative) peak value

The methods here are, as described, valid for static structures and do not take dynamic response into consideration.

Quasi-steady method

The central assumption in the quasi-steady method is that the actions on the building respond to turbulence as if it was a steady change to the wind speed and direction (Cook, 1990, p. 20). In its most simplified form, the wind action is constantly proportional to the dynamic wind pressure exerted on the building, that is:

$$q_w = \bar{c}_p \cdot q_b(z) \quad (2.3)$$

where

$$q_b(z) = \frac{\rho}{2} \hat{V}^2(z)$$

The wind pressure, in other words, equals the mean pressure coefficient times the dynamic wind pressure induced by the gust speed at the reference height above ground. This

2. Review of products and research

assumption is correct when the size of the turbulence eddies are comparable to the size of the building, however, since turbulence induced by the building itself is ignored, this method will underestimate local wind actions on smaller building features (because the loading coefficient is averaged over time). The quasi-steady method for determining loading coefficients is therefore unsuitable for determining wind loads on roof-mounted solar panels (Lieb, 2009).

Peak-factor method

The peak-factor takes turbulence induced from the airflow deflection of the structure into consideration by including the root-mean-square deviation from the mean pressure coefficient, c'_p , in the resulting pressure coefficient (Lieb, 2009). The resulting loading coefficient, shown in (2.4). The *peak factor*, $g(t)$, can be described as a function of the wind turbulence frequencies in the boundary layer and around the structure (Cook, 1990, p. 25).

$$\hat{c}_p = \bar{c}_p + g(t) \cdot c'_p \quad (2.4)$$

and for the largest negative pressures

$$\begin{aligned} \check{c}_p &= \bar{c}_p - g(t) \cdot c'_p \\ q_w(z) &= \hat{c}_p \cdot \frac{\rho}{2} v_{10,min}^2 \end{aligned} \quad (2.5)$$

The resulting wind load q_w is determined using the 10-minute average wind speed in Eqn. (2.5) (Lieb, 2009, p. B4).

Extreme-value method

Cook (1990) describes one further method, used in the studies by Geurts, Ravenhorst, and Donkervoort (2002), Blackmore (2004) and thus creating the foundation for the NVN 7250 (Nederlands Normalisatie-instituut, 2007) used later in this study. While both the quasi-steady method and the peak-factor method determines the extreme pressures using time-averages, the extreme-value method observes extreme actions (largest positive and negative pressures) as statistically independent events and uses a statistical distribution function to predict the peak pressure coefficients \hat{c}_p and \check{c}_p with the desired exceedence probability, $P_{\hat{c}}$ and $P_{\check{c}}$, respectively (Cook, 1990, p. 36).

The extreme values \hat{c}_p and \check{c}_p consist of peak pressures averaged over the smallest load duration t , that is, the longer t is, the more load peaks are equalized and the peak values approaches the mean pressure coefficient. The load duration t indicates the duration of the shortest wind gust that induces simultaneous loading on the entire structure under consideration. The extreme values follows a so-called Fisher-Tippet Type I distribution, from which extreme values of the desired probability can be extrapolated. Fitting the distribution parameters to the data, extreme values of desired probability can be derived through their cumulative distribution function.

Smallest load duration

Transient loads or wind gusts shorter than a certain duration t will not be able to load the entire structure or part of structure under consideration at a time, and are thus not to be considered when determining the peak pressures. For the peak-factor method, this duration is used as a low-pass filter for the wind speed or pressure variations when determining the peak factor g (Cook, 1990, p. 27). For the extreme-value method, the duration t is the time over which a peak load must be averaged (Cook, 1990, p. 33). The smallest load duration can be determined with the following expression:

$$t\bar{V} = 4.5l \quad (2.6)$$

In Equation (2.6), \bar{V} denotes the mean wind speed, while l represents the “effective size parameter for the structure or part of the structure” (Cook, 1985, p. 277). In short, this parameter depends on the structure geometry and the action on the structure being considered; for example, if the overturning moment from wind action on a cantilever is the action considered, l corresponds to the effective lever of the resulting moment-inducing wind force acting on the structure (Cook, 1985, p. 186).

Synthesizing local loading coefficients to global

When integrating the cladding pressures to obtain the resulting load coefficients \hat{C}_p and \check{C}_p for an entire structure (e.g. for bracing design), the problem of correlation between peak pressures arises: Local extreme pressures (corresponding to \hat{c}_p or \check{c}_p) might not develop simultaneously over the building. The solution suggested by Cook (1990, p. 32–33) is to add the minimum extreme $\check{c}_{p,i}$ when $\bar{c}_{p,i} < 0$ (that is, local mean pressure is **negative**) and the maximum $\hat{c}_{p,i}$ when $\bar{c}_{p,i} > 0$ (local mean pressure **positive**). It is however also important to notice *which* action is being integrated when applying this procedure. The general notion should be: Does the local action increase or reduce the global action? (Cook, 1990, p. 27). For illustrative purposes, the integration procedure is described as a formula in Equation (2.7) along with Figure 2.7.

$$\hat{C}_p = \frac{1}{\sum A_{ref,i}} \left(\sum_{\bar{c}_{p,i} \geq 0} \hat{c}_{p,i} \cdot A_{ref,i} + \sum_{\bar{c}_{p,i} < 0} \check{c}_{p,i} \cdot A_{ref,i} \right) \quad (2.7)$$

2.3. Wind load investigation

Existing design guidelines and published studies on wind actions on photovoltaic modules are reviewed in this section. A principle for applying the wind loads to the mounting systems in the static model is conceived, and the geometrical parameters of mounting systems and the underlying building are reviewed with respect to coverage in the existing research.

2. Review of products and research

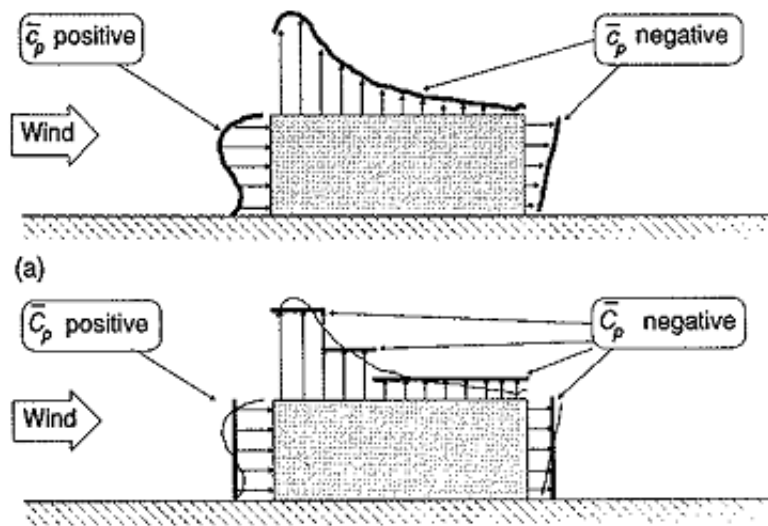


Figure 2.7.: Wind pressure integration to create global loading coefficients (Cook, 1990, p. 13).

2.3.1. Current construction standards

As of September 2010, the current standards for wind actions are the Eurocode 1: *Actions on structures – General Actions – Part 1-4: Wind Actions* (European Committee for Standardization, 2005), commonly referred to as *EN-1991-1-4*, DIN 1055 *Einwirkungen auf Tragwerke – Teil 4: Windlasten* (Deutsches Institut für Normung, 2005) and *Boverkets handbok om snö- och vindlast, BSV 97*, (Boverket, 1997), valid in Germany, the Eurocode area, and Sweden respectively. Neither the EN 1991-1-4 nor the DIN 1055-4 provides wind load coefficients for solar collectors on flat roofs (Blackmore, 2004; Ruscheweyh and Windhövel, 2009).

A common approach has been to use the load coefficients for flat roofs or duo-pitched roofs given in these standards (Ruscheweyh and Windhövel, 2005). However, the values provided do not describe the actual flow conditions very well, often overestimating the wind action, sometimes underestimating the actions in roof edge areas. This causes the dimensioning using existing standards to be largely uneconomical and sometimes insecure, which makes this approach undesirable (Ruscheweyh and Windhövel, 2005).

2.3.2. Previous investigations of wind loads

Only a handful of investigations into the wind loads on solar collectors on flat roofs has so far been made, none of which comprehensive enough to create a method for assessing the wind loads rooftop-places panels on arbitrary buildings. However, due to the increased interest in solar energy in western Europe, a pre-standard is being developed in the Nether-

lands, the NVN 7250 (Nederlands Normalisatie-instituut, 2007).

Radu, Axinte, and Theohari (1986) performed a wind tunnel study of a larger flat-roofed building with inclined solar panels on the roof in two configurations; single- and dual-row mounting systems. The model was placed on a turntable in order to investigate all wind directions, in boundary-layer flow. Net wind pressure coefficients were calculated for each panel individually and for each row as a peak average. Shielding effects from the edge rows were also noted. Radu and Axinte (1989) investigated the effects from roof parapets on wind loads on flat-roof-mounted panels, where both wind suction and pressure were found to be significantly reduced, especially on roof edges and corners. For the first, wind-facing row, the pressure forces on roof-mounted panels on a five-story building were reduced with 45 %, and the uplift was reduced with 25 %. The reduction was smaller when the building height was increased.

Wood, Denoon, and Kwok (2001) investigated a flat-roofed building with solar collectors parallel to the roof surface. The distance between roof cladding and panels, as well as the lateral distance between the panel rows were varied, but neither was found to have considerable effect on the resulting wind loads on the panel. Instead, proximity to the leading edge and the orientation of the panels towards the wind direction are shown to have larger influence. Wood et al. also considers the impact on the building and the possibility of changed wind loads from adding the solar collectors.

The most comprehensive study to this date was done by Geurts, Ravenhorst, and Donkervoort (2002), in which wind pressures are measured on panels on a rectangular building in boundary-layer flow. Panels and pressure taps are placed on the roof, and the supporting structures are modeled both as “open” and “closed” (refer to Sections 2.1.1 and 2.1.3, respectively), where the sides of the structures are covered. Measurements were done without parapet on the roof edge, and with a relatively small one, approx. 200 mm to scale. Blackmore (2004) published design guidelines for roof-mounted solar panels based on this study. The chosen wind load coefficients are the most conservative found by Geurts, and Blackmore does not take into account that different wind load maxima appear under different wind attack angles. Geurts, van Bentum, and Blackmore (2005) and Geurts and van Bentum (2007) also compiled these results into design guidelines for Dutch conditions, which have since been adapted for the Dutch pre-standard *Nederlandse voornorm NVN 7250 Zonne-energiesystemen – Integratie in daken en gevels – Bouwkundige aspecten* (Nederlands Normalisatie-instituut, 2007), referred to as NVN 7250.

The Dutch prestandard NVN 7250 consolidates the investigations in the previous paragraph and provides design rules, wind load coefficients, and structural details for roof-mounted panels. Advice is also given for inclined roofs. Wind load coefficients are, like above, provided for open and closed structures, however not separated according to wind direction. NVN 7250 limits the described cases to isolated, rectangular buildings, with panels parallel to the walls. Approaches are given for buildings with flat roofs of different heights, and for roofs with lanterns, where the panels experience increased loads just below the height difference.

Outside of the concerted NVN 7250 effort, Ruscheweyh and Windhövel (2005, 2009) have published two studies for larger industrial roofs. The wind actions measured and

2. Review of products and research

the resulting wind loading coefficients presented in these studies are significantly smaller than those presented in the NVN 7250, however, the authors notes that these loads and loading zones for the roofs are very specific to the structure geometries described in the studies. In these studies, the wind direction is taken into consideration when calculating uplift forces. The way the wind loads are modeled, only the modules along the north faces of the buildings experience larger uplift forces. The wind loads are also divided into a stationary part, and a dynamic part. The dynamic part is used for dimensioning the mounting system, and (spread out over a larger surface) for uplift force dimensioning. For assessing the overall impact on the building and rooftop, only the static part is considered.

Further, Ruscheweyh and Windhövel (2009) conclude that the horizontal reaction forces of the solar collectors measured in wind tunnel tests are significantly smaller than those derived by integrating the pressure on the panels. Through the spatial variations of the wind pressure at each given time point, the resulting horizontal force to be absorbed by the building's wind bracing is "clearly smaller" (p. 187) than the sum of the peak loads onto each panels. No estimation is given for this reduction, though.

2.3.3. Summary with respect to geometrical parameters

The findings from the previous research is summarized with regard to the different geometrical parameters, to possibly exclude parameters that have been investigated.

Influence from structure geometry

None of the so far mentioned research investigates the effects of the mounting system's geometrical properties, other than being "open" (module exposed to wind forces from all directions) and "closed" (only the active face of the module is exposed to wind forces). Geurts, van Bentum, and Blackmore (2005) suggests that the wind pressure coefficients given in their report are suitable for a module pitch between 10 and 40 degrees, although the tests by Geurts, Ravenhorst, and Donkervoort (2002) were done with a module pitch of 35 degrees. Other values are given for pitches below 10 degrees, and pitches between 40 and 70 degrees. The wind load coefficients given by Blackmore (2004) are claimed to be valid between 25 and 45 degrees' pitch. Ruscheweyh and Windhövel (2009) likewise note that the wind load decreases with a more gentle slope of the module.

Influence from building geometry

The reports by Geurts et al., Geurts & van Bentum, and Blackmore, all suggest an approach where the roof of a rectangular building is divided into wind loading zones similar to those in EN 1991-1-4, which results in corner, edge, and center loading zones (this principle is shown in Figure 2.8). Wind load coefficients are then given for support structures in these zones separately. Thus wind loads for all isolated, rectangular buildings can be investigated. Load coefficients are given for open and closed supports, with separate values for roofs with a parapet higher than 200 mm.

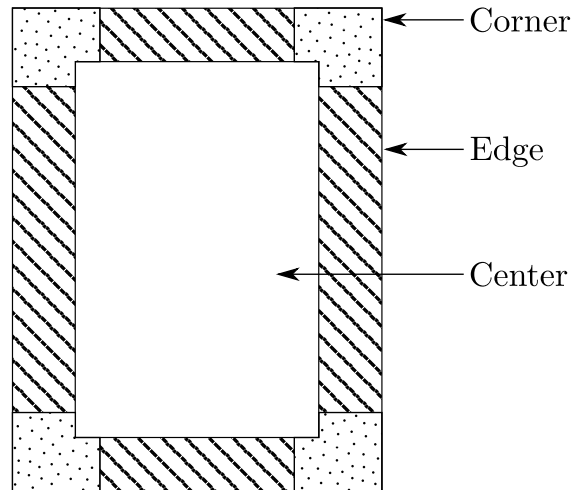


Figure 2.8.: Load zone principle on flat roofs according to NVN 7250 (Illustration by author)

Ruscheweyh and Windhövel instead suggest a division of the roof where the only north-facing edges experience large uplift forces, and only the south-facing are exposed to larger pressure, see Figure 2.9 (left and right, respectively). Since the modules are directed towards the south, this means that only northern winds can attack the panels from behind to create the largest uplift forces. The outer panels along the southern edges are then shielded from the flow. The difference between these approaches are to be investigated in subsequent parts of this thesis. With southern wind flows, the downwards pressure is larger along the southern edge of the building.

Further, higher buildings tend to create a shielding effect of the leading edge, reducing the loads on the wind-facing collector rows compared to squatter buildings, since the modules are smaller relative to the underlying building influencing the wind streamlines (described briefly by Ruscheweyh and Windhövel, 2005). This is not taken into consideration in any design guidelines.

Influence from parapets:

Radu and Axinte (1989) found a strong reducing effect on the panels' wind loads from larger parapets (height 1 m, varying permeability). The effect diminishes as the building gets higher, and the results for all combinations of building height and parapet are not presented, which makes it hard to reuse these results.

Geurts, van Bentum, and Blackmore (2005) claims a significant influence on the loads on open support structures, even with a lower parapet (200 mm), while the effect on closed structures is not significant, although separate coefficients for both cases are given for both kind of structures. Additional values for higher parapets are not given. This distinction is maintained in the NVN 7250.

2. Review of products and research

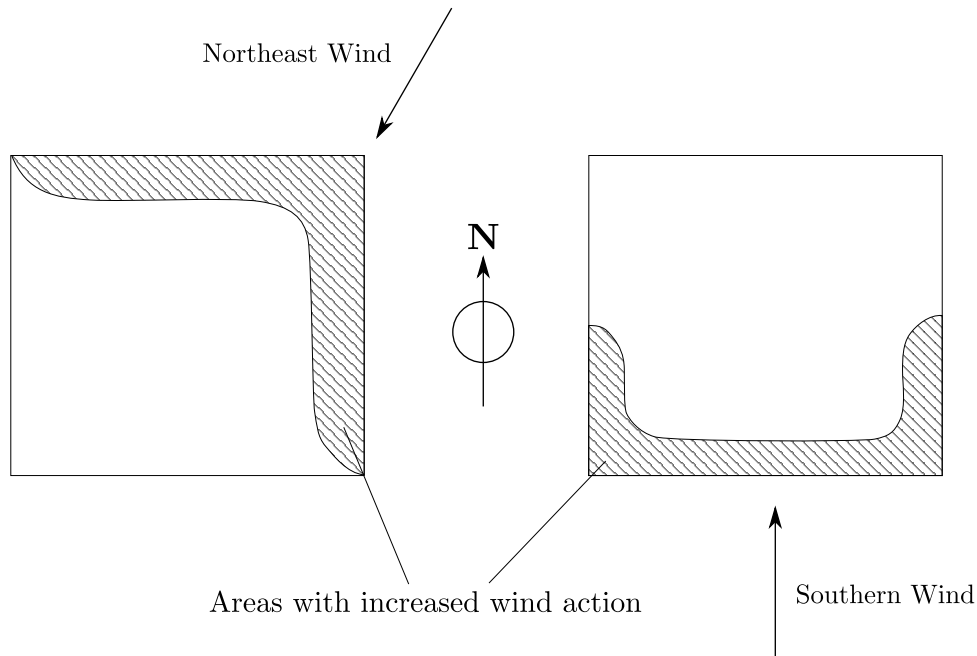


Figure 2.9.: Load zones on flat roofs according to Ruscheweyh and Windhövel (2009), principle (Illustration by author)

Influence on wind forces from module arrangement on building.

Wood, Denoon, and Kwok (2001) concludes that the lateral distance between the panel rows has no effect on the wind loads. It should be noted that the panels were kept relatively concentrated on the roofs.

On the other hand, Radu, Axinte, and Theohari (1986) as well as Radu and Axinte (1989) keeps the panels in two groups, and notes that the panels shelter the inner rows, while the outer are more exposed to wind forces. The NVN 7250 also provide different wind coefficients for protected and unprotected panel rows, though this effect is only accounted for in the central load zone of the roof. No investigations of the effects of roof installations (chimneys, skylights, antennas), and irregular spacing caused by these, were found.

Influence from solar collectors on building

Wood, Denoon, and Kwok (2001) concludes that to calculate the net additional wind load on the roof cladding, the topside pressure on the panels should be compared to the pressure on the roof without panels, since the pressure on the lower side of the panel equals the pressure on the roof cladding, which means that they will cancel each other out in terms of net load on the roof. Topside pressure or suction was always lower than the pressure or suction without panels, except for at the very leading edge of the building, which means that the wind on the panels doesn't increase the net wind load on the roof. The load capacity of the roof needs to be verified for a combined load case with line loads from the

panel supports and distributed loads from the forces acting on the roof. The panels also induce horizontal reactions which further induce loading on the buildings wind bracing, as noted by Ruscheweyh and Windhövel (2009).

2.3.4. Conclusions from previous research

For simple cases, the guidelines found in the previous paragraphs can be used for determining wind loads, though in most cases, further research is needed. The findings from this section is used to create a static model of the mounting system in Chapter 3, and to create adaptations of the wind actions to the geometries processed in Chapter 4.

Investigated parameters

The wind loads on panels can only be roughly estimated through the current guidelines. For rectangular buildings of arbitrary height, the NVN 7250 gives a first estimation, and it is the aim of the following chapters to discuss a few approaches for estimating the wind loads on roofs not explicitly covered by this document. By separating the panels into shielded and unshielded positions, the Dutch pre-standard also accounts for effects by gaps in the module rows. Whether or not this is sufficient, is to be seen in the dissertation.

Wood et al. suggests that the lateral distance between panels has little to no influence on wind loads, neither on panels nor on the roof cladding. This parameter does not need to be investigated, providing that the distances are sufficiently small to shield the downstream rows. Wood also suggests that the only additional net load being brought onto the underlying building is the dead weight of the solar collectors and their ballast, which simplifies the verification of the building's remaining load capacity.

The conclusion being drawn here is to use the NVN 7250 as origin for the wind load assessments suggested in later chapters, since it is the most comprehensive and detailed guideline found for the structures being discussed.

Suggestions for future research

Just because a parameter is neglected in the design guidelines, does not mean that it has no influence. Examples of this is the distance between roof edge and first panel row, the relation between solar collector height and overall building height, and mounting system geometry. Further, the only one of the above referred investigations that investigates panels oblique to the walls of the rectangular building is the one by Ruscheweyh and Windhövel (2005). No comparison between oblique and parallel panel rows is made in this study. All of the above mentioned factors need to be investigated.

Radu, Axinte, and Theohari (1986) calculated peak wind pressures averaged over entire panel rows. The coefficients were significantly smaller than the local peak pressure coefficients based on one panel each, since the wind pressure on a surface varies in space at all times. The larger the surface is that is being considered, the more unlikely that peak pressure occurs over the entire surface at once. When module surfaces grow bigger and the panel rows are laterally connected, provided that the connections are rigid enough,

2. Review of products and research

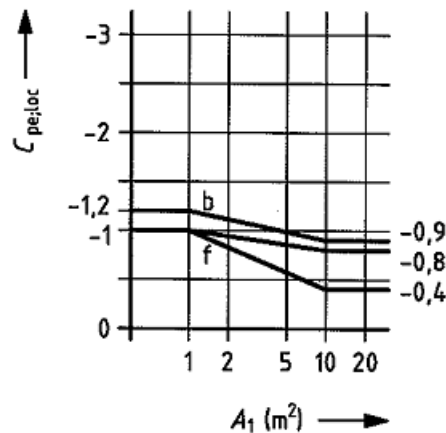


Figure 2.10.: Local wind pressure coefficient diminishing when considering a larger area (Nederlands Normalisatie-instituut, 2007, Figure A.2a).

one only has to consider the static equilibrium of the entire structure. Since peak loads decrease with an increase in averaging surface, this could provide for a more economical wind load dimensioning, and thus make solar panels on roofs with smaller load reserve feasible. This is also suggested by Figure 2.10, where smaller wind load coefficients are given when larger surfaces are considered at once.

Finally, Radu & Axinte concludes in their 1989 study that parapets have a large influence on the wind loads, while Geurts, Ravenhorst, and Donkervoort (2002) and subsequent publications notes a load reduction by 20 % for the edge zones with open structures, but notes no significant reduction in the central loading zone and none at all for closed structures. This is an interesting question since it would reduce the wind loads in the most exposed areas and thus even out the ballast distribution on the roof.

Conclusions for creation of static model

Using the approach to wind loads shown in Section 2.3.3, it is shown in Figures 2.8 – 2.9 that the wind load will vary in the longitudinal direction of the mounting system, when a connected mounting system crosses one or more loading zones (see Figure 2.8). The static model needs to allow for this. Further, Figure 2.11 shows how the wind load (as a principle) varies across the panel surface, according to the NVN 7250 (left) and Ruscheweyh and Windhövel (2005) on the right. Thus, the static model needs to allow for wind load variations in the transversal direction of the mounting system.

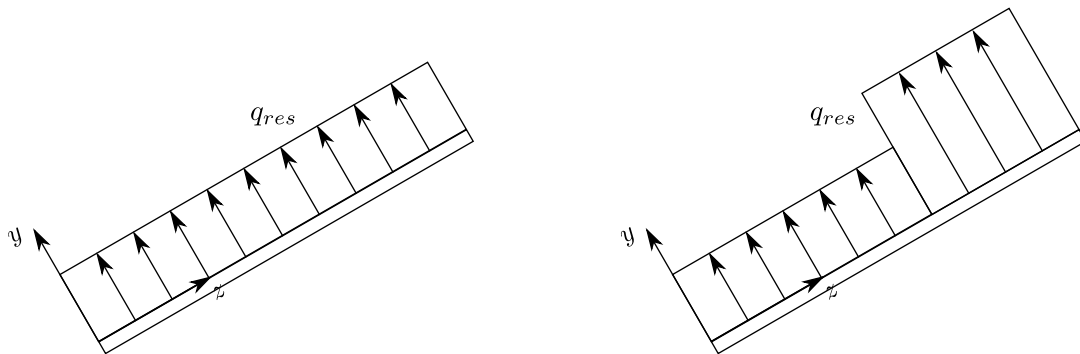


Figure 2.11.: Wind load distribution on panel section according to *NVN 7250* (left) and Ruscheweyh and Windhövel (2005) (right) (Illustration by author}

3. Loads and statics

The outer actions and internal action state of the mounting system is here being systematized using the conclusions from the product research (regarding geometry, Section 2.1.6) and the approach to wind loads (Section 2.3.4).

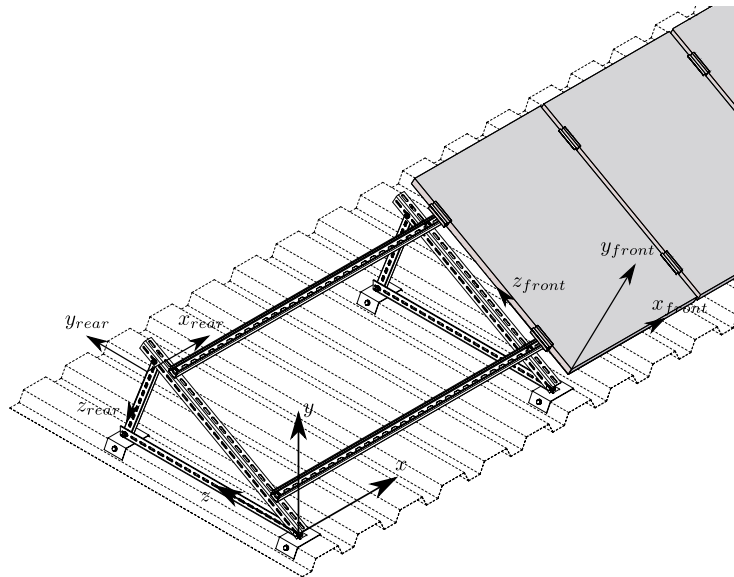


Figure 3.1.: Isometric view of the structure being modeled, with global and local coordinate systems (showing positive directions, rather than origins)

3.1. Description of structure

The structure being considered here is a simple frame out of sheet-metal steel profiles, for the purpose of mounting solar collectors onto flat roofs, as shown in Figure 3.1. The structure might have an arbitrary number of panel rows, and an arbitrary length in the x direction. The panels can be placed vertically or horizontally. In the latter case, the inner longitudinal beams are shared between panels if there are multiple rows. The triangular substructures are placed with an arbitrary distance, however, the cantilevers on each end are kept symmetrical. The structure and the local elements are provided with global and local coordinate systems, to assign positive directions of loads and geometrical coordinates.

3. Loads and statics

In order to change the aerodynamic behavior of the structure, its rear face can be closed off with a panel, usually a thin metal sheet. The static model must also take the existence of such a surface into account.

3.1.1. Actions on structure

The actions on the structures discussed here and their dimensioning combinations are derived in the following sections.

Actions

The loads under consideration are the dead weight of the panels, snow loads, and wind loads. The two first are easily determined through the panel fact sheet, and the snow load standards for the respective country, see Figure 3.2

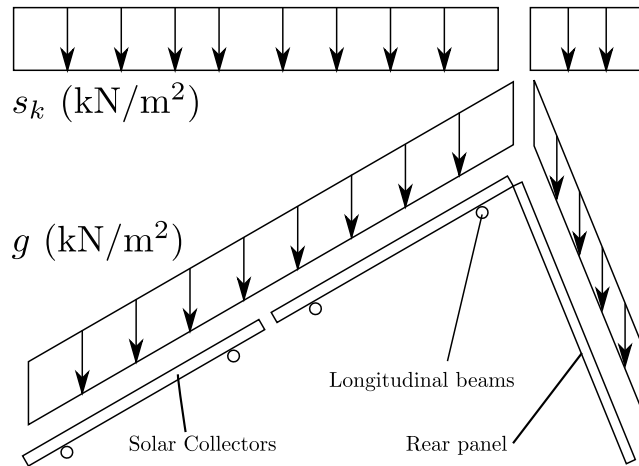


Figure 3.2.: Snow and dead load acting on structure

The dynamic wind pressure is determined by the height above ground of the upper edge of the structure. Variations in the wind load acting on the solar collectors are allowed both in the longitudinal (x_{front}) direction and in the transversal (y_{front}) on the front face, but only in the longitudinal direction (x_{rear}) on the rear face, see Figure 3.3. The latter assumption is made since all the wind load approaches investigated in this study assumes loads on the rear face constant in transversal direction.

Heterodynes for dimensioning

The load combinations used for dimensioning are shown in Table 3.1, as derived from the Eurocode 0 (European Committee for Standardization, 2002). Combinations 3–5 are derived for the ultimate limit state **STR**, *Internal failure or excessive deformation* (Paragraph 6.4). Load combinations are also given for the ultimate limit state **EQU**, *Loss of static equilibrium of the structure or any part of it considered as a rigid body*, where the permanent

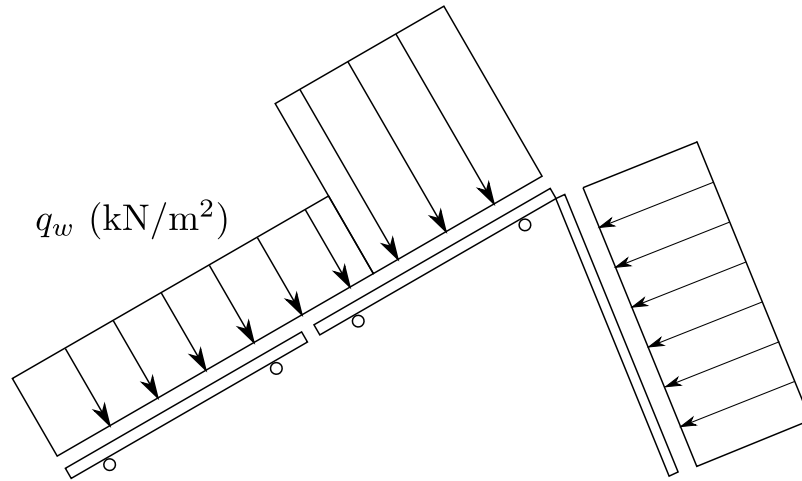


Figure 3.3.: Wind loads on structure

action from the structure's weight is reduced since it has a favorable effect. In this study, the EQU load combination from the NVN 7250 is used instead; see Section 4.1.5 for a rationale.

Table 3.1.: Load combinations for dimensioning, according to European Committee for Standardization (2002).

Heterodyne	γ_G	γ_{Wind}	γ_{Snow}
3. Wind upwards	1.0	-1.5	0
4. Wind downwards	1.35	1.5	1.05
5. Snow	1.35	0.9	1.5

The combinations of wind suction and pressure on the front and rear panel must be verified separately when a rear panel is present, depending on wind direction. That means that there are 2 subcases for the third heterodyne on a structure with rear panel (Ruscheweyh and Windhövel, 2009).

1. Pressure on the front, suction on the rear, wind from the south (Figure 3.4a)
2. Suction on the front, pressure on the rear, wind from the north (Figure 3.4b)

Transitions of loads onto structure

The surface loads onto the solar collectors (including dead load) are projected as line loads onto the longitudinal beams. The loads parallel to the surface are divided evenly, however, the perpendicular loads may distribute differently since they are allowed to vary in the

3. Loads and statics

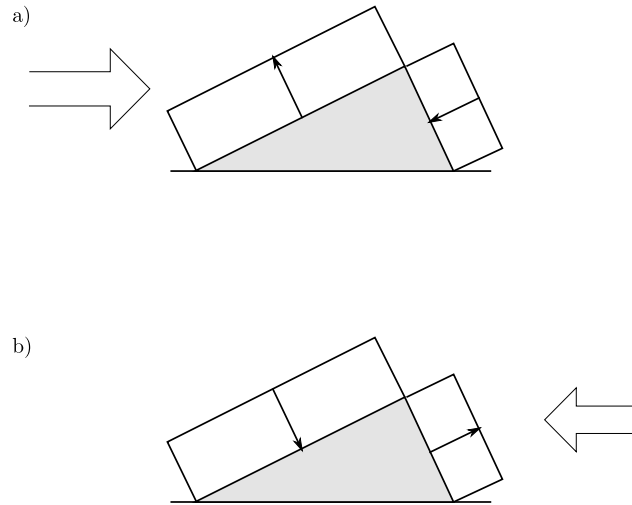


Figure 3.4.: Combinations of suction and pressure depending on wind direction (Illustration by Author)

across direction of the panel surface. The distribution of the loads is presented in Figure 3.5.

The photovoltaic modules are actually mounted with clamps onto the longitudinal beams, causing concentrated actions. The loads from the modules are however treated as line loads, since each load is small and the longitudinal beams are long compared to the single modules.

3.2. Section forces

In the following sections, it is shown how to determine the section and reaction forces of a mounting system within the constraints given in the previous paragraphs. The models are kept as general as possible, to yield correct results for any load and geometrical input.

3.2.1. Longitudinal beam

The longitudinal beams of the structure are continuous over an arbitrary number of supports N , with constant cross section and with loads varying along their x -axis (Figure 3.6). The considered load case, as shown in previous sections, is a varying, though section-wise constant, line load, as shown in Figure 3.6. The *Flexibility Method* (Germ. *Kraftgrößenverfahren*), as described by Meskouris and Hake (1999), is used to determine the section forces and the reactions.

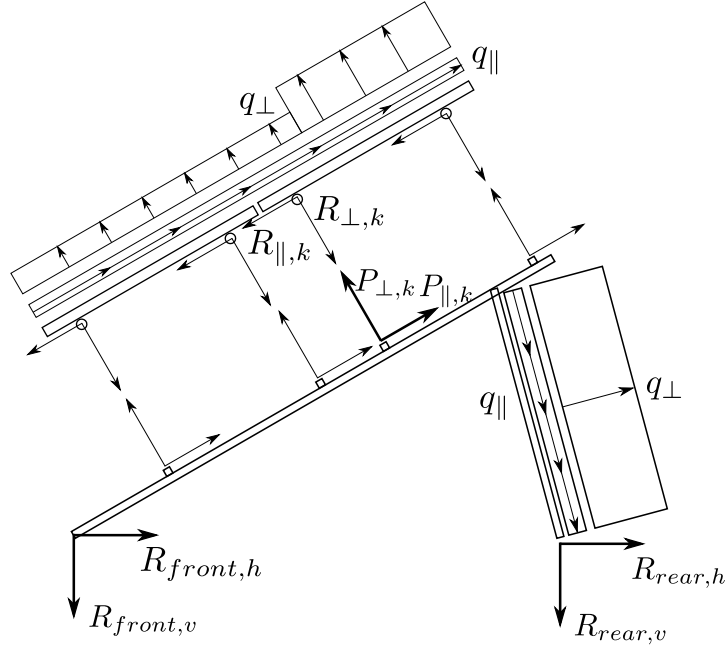


Figure 3.5.: Distribution of loads from panels onto mounting system

Principle for determining section forces

The statically indeterminate beam is simplified to a simply supported beam by removing the middle supports $2 - [N - 1]$ (Meskouris and Hake, 1999). This system is called the *primary determinate structure* (Germ. *statisches Grundsystem*), and is shown in Figure 3.7. The deflections at the removed supports from the outer loads, $\delta_{2,0} - \delta_{N-1,0}$ (shown in Figure 3.10), are determined. Since the original system has supports in these positions, it is known that the deflection in these points has to be *zero*, that is, for each point of support:

$$\delta_{n,0} - \sum_{i=2}^{N-1} X_i \cdot \delta_{n,i} = 0 \quad (3.1)$$

With the help of equation (3.1) an equation system can then be formed:

$$\begin{bmatrix} \delta_{22} & \dots & \delta_{N-1,2} \\ \vdots & \ddots & \vdots \\ \delta_{2,N-1} & \dots & \delta_{N-1,N-1} \end{bmatrix} \begin{bmatrix} X_2 \\ \vdots \\ X_{N-1} \end{bmatrix} = \begin{bmatrix} \delta_{20} \\ \vdots \\ \delta_{N-1,0} \end{bmatrix} \quad (3.2)$$

By calculating the deflection at each inner support i from a *unit load* $P = 1$ kN at each support n , an equation system can be created (see Equation (3.2)) for determining the reaction forces at the removed supports. The outer reaction forces at support 1 and support N can then be determined from static equilibrium. Finally, the bending moment

3. Loads and statics

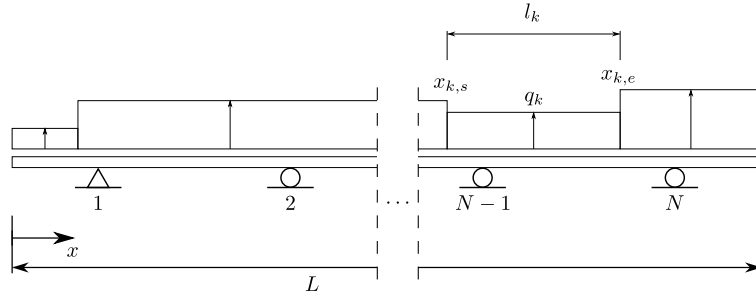


Figure 3.6.: The longitudinal beam with loads

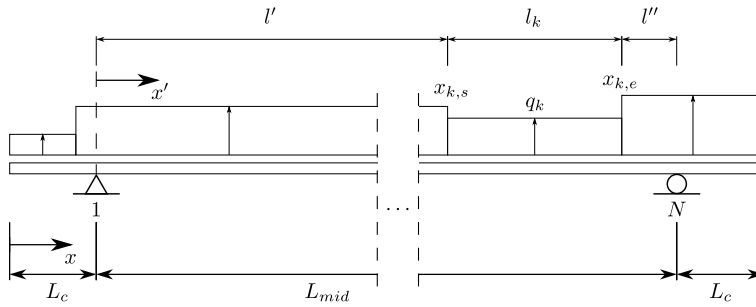


Figure 3.7.: Primary determinate structure

distribution is determined by superpositioning the outer loads with the reactions at the inner supports.

Section forces of the primary determinate structure

The section forces of the primary determinate structure is determined by dividing the loads on the beam into elementary load cases, as described by Isaksson and Mårtensson (2006). Loads applied to the cantilevers of the beam are separated for loads acting on the mid section, since they constitute separate elementary load cases. The resulting bending moment is determined by superpositioning all loads affecting the system:

$$M_0(x) = \sum_k M(q_k, x) \quad (3.3)$$

Load applied to cantilever: Considered here is a constant line load, beginning somewhere on the left cantilever and ending before the first support (see Figure 3.8). Before the load is applied, there are no section forces:

$$x \leq x_{k,s} \quad : \quad M(x) = 0 \quad (3.4)$$

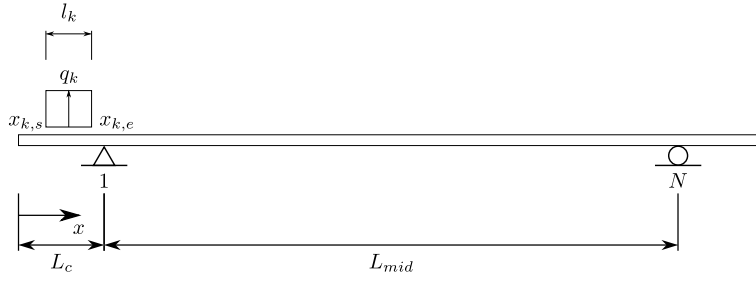


Figure 3.8.: Load case and notation for system w. load on cantilever

As the load applies, the bending moment grows quadratic:

$$x_{k,s} < x \leq x_{k,e} \quad : \quad M(x) = q_k \frac{(x - x_{k,s})^2}{2} \quad (3.5)$$

The bending moment then increases linearly until the first support:

$$x_{k,e} < x \leq x_1 \quad : \quad M(x) = q_k \cdot l_k (x - x_{k,s} - l_k/2) \quad (3.6)$$

After the first support, the bending moment decreases linearly to zero after the last support:

$$M(x_1) = q_k \cdot l_k (L_c - x_{k,s} - l_k/2)$$

$$x_1 < x \leq x_N \quad : \quad M(x) = M(x_1) \cdot \left(1 - \frac{x - L_c}{L_{mid}}\right) \quad (3.7)$$

$$x_N < x \quad : \quad M(x) = 0 \quad (3.8)$$

Section forces from loads applied to the right cantilever follow the same formulas, though with a mirrored coordinate system.

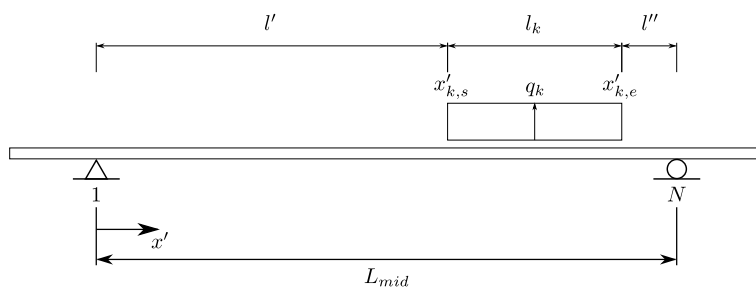


Figure 3.9.: Primary determinate structure with load on mid field

Load applied to mid section Consider a constant line load, applied to a *part* of the mid section, as pictured in Figure 3.9. The load q_k is constant, beginning at the position $x_{k,s}$

3. Loads and statics

and ending at $x_{k,e}$. The bending moment can then be described as follows (note that an alternative coordinate system, $x' = x - x_1$, is introduced to simplify the expressions):

$$x' \leq 0 \quad : \quad M(x') = 0 \quad (3.9)$$

$$0 < x' \leq x'_{k,s} \quad : \quad M(x') = \frac{q_k \cdot l_k \cdot \left(\frac{l_k}{2} + l''\right) \cdot l'}{L_{mid}} \frac{x'}{l'} \quad (3.10)$$

$$x'_{k,s} < x' \leq x'_{k,e} \quad : \quad M(x') = q_k \left[\frac{l_k \left(\frac{l_k}{2} + l''\right)}{L_{mid}} \cdot x' - \frac{(x' - l')^2}{2} \right] \quad (3.11)$$

$$x'_{k,e} < x' \leq x'_N \quad : \quad M(x') = \frac{q_k \cdot l_k \cdot \left(\frac{l_k}{2} + l''\right) \cdot l''}{L_{mid}} \left(1 - \frac{x' - l' - l_k}{l'} \right) \quad (3.12)$$

$$x'_N < x' \quad : \quad M(x') = 0 \quad (3.13)$$

Bending moment from reaction forces: The load from the support reactions at the inner support corresponds to a concentrated load on a simply supported beam, the section forces are easily calculated (note that here, once again, is the translated coordinate system $x' = x - x_1$ used). The formulas in this section are also used to determine the virtual load state \overline{M}_i used in equation (3.18) to calculate beam deflections. In these cases, $P_k = 1$ kN for all values of k .

$$x' \leq 0 \quad : \quad M(x') = 0 \quad (3.14)$$

$$0 < x' \leq x'_k \quad : \quad M(x') = \frac{P_k \cdot (L_{mid} - x'_k)x'}{L_{mid}} \quad (3.15)$$

$$x'_k < x' \leq x'_N \quad : \quad M(x') = \frac{P_k x'_k (L_{mid} - x')}{L_{mid}} \quad (3.16)$$

$$x'_N < x' \leq L \quad : \quad M(x') = 0 \quad (3.17)$$

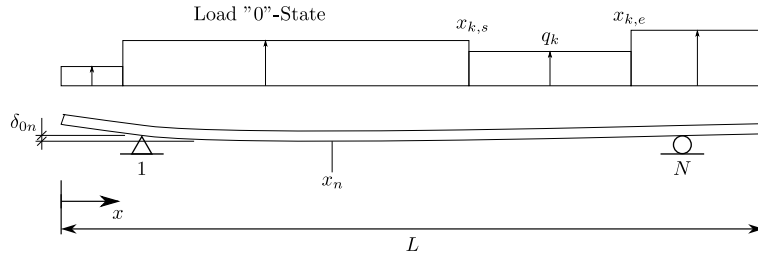


Figure 3.10.: Notations for deflection from load on the primary determinate structure

Determining the support deflections from applied loads

The deflections at the supports are calculated using the *principle of virtual forces* (German: *Prinzip der virtuellen Kräfte*), as described by Meskouris and Hake (1999). The deflection at point x_n is determined as follows:

$$\delta_{0n} = \int_0^L \overline{M}(x) \cdot \frac{M_0(x)}{EI} dx \quad (3.18)$$

In equation (3.18) \overline{M} represents the bending moment at position x , caused by a unit load $F_n = 1$ kN being applied at the point x_n , while M_0 is the bending moment from the live loads applied to the primary determinate structure.

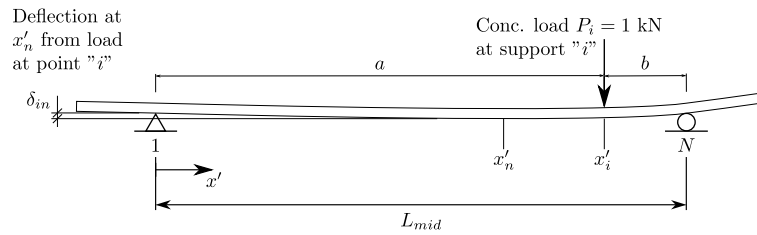


Figure 3.11.: Notations for deflections from support reactions

Determining deflection at supports, from support reactions

The system stiffness matrix is created by calculating the deflections from each support n caused by unit forces $P = 1$ kN at each support i , for all combinations of n and i . Since this is an elementary load case, Isaksson and Mårtensson (2006) provides expressions for the deflection of the beam at each point:

$$x'_n \leq x'_i : \quad \delta_{in} = \frac{PL_{mid} \cdot bx'_n}{6EI} \left(1 - \frac{b^2}{L_{mid}^2} - \frac{x'^2}{L_{mid}^2} \right) \quad (3.19)$$

$$x'_n > x'_i : \quad \delta_{in} = \frac{PL_{mid} \cdot a(L_{mid} - x'_n)}{6EI} \left(\frac{2x'}{L_{mid}} - \frac{a^2}{L_{mid}^2} - \frac{x'^2}{L_{mid}^2} \right) \quad (3.20)$$

By combining all support positions $2 - [N - 1]$ with all load positions $x_2 - x_{N-1}$, the left side of the equation system (3.2) is created.

Reaction forces

The reaction forces on the inner supports are determined by solving the equation system (3.2). It is then trivial to determine the reactions at the outer supports by applying static equilibrium. The rightmost support reaction is determined through moment equilibrium around the leftmost support (3.21), the leftmost reaction then via vertical equilibrium (3.22).

3. Loads and statics

$$\curvearrowright \quad X_N = \left(\sum_{k=1}^n q_k \cdot l_k \left(x'_{k,s} + \frac{l_k}{2} \right) - \sum_{k=2}^{N-1} x'_k \cdot X_k \right) \frac{1}{x'_N} \quad (3.21)$$

$$(\uparrow) \quad X_1 = \sum_{k=1}^n q_k \cdot l_k - \sum_{k=2}^N X_k \quad (3.22)$$

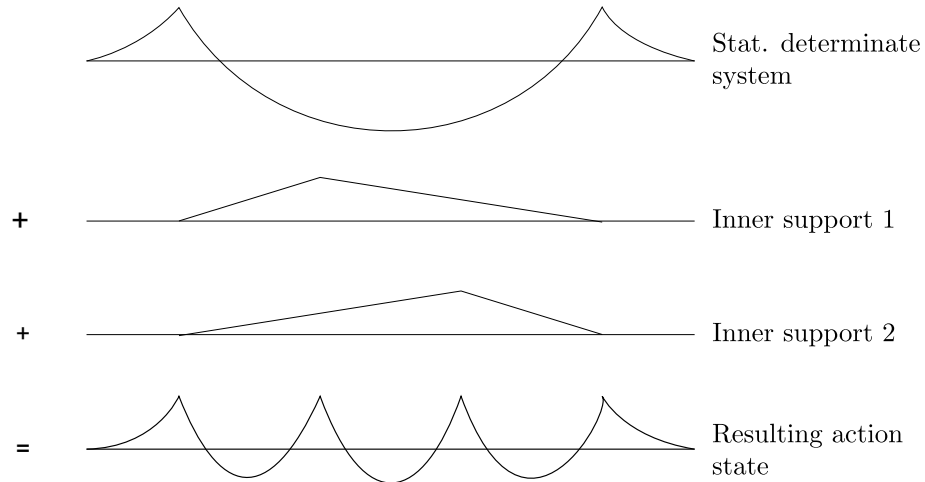


Figure 3.12.: Superpositioning of moments from loads and reactions

Bending moment distribution

The resulting bending moments are determined by summing all section forces from outer actions and from reaction forces, according to Figure 3.12. The process described above is done for all load cases, with loads in y - and z -direction treated separately.

Summary – Longitudinal beam

A short summary of the process to determine the section forces of the longitudinal beam, and the reactions acting on the triangular substructure:

1. Simplify the statically indeterminate structure to a *primary determinate structure*.
2. Calculate the internal action state from the real actions on the structure
3. Determine the deflection at each removed support, using the section forces from step 2.
4. Determine the deflection at each removed support j from a unit load applied at each support i .

5. Solving the equation system given in step 3 (right side) and 4 (system matrix), as shown in Equation (3.2), gives the removed support reactions. The remaining support reactions are determined through static equilibrium. The support reactions are the actual forces acting on the *triangular substructures*, described in Section 3.2.2.
6. Determine the bending moment from the inner support reactions.
7. Superpositioning the results from point 2. and point 6. gives the resulting internal action state of the original structure.

3.2.2. Triangular Substructure

The longitudinal beams rest upon a triangular substructure. Both corners rest on fixed hinges, unable to move in horizontal and vertical direction. The longer, more gentle sloped beam is below called the *transversal beam*, and the steeper element is called the *rear beam*. The actions on the triangular substructure are divided into four elementary cases, for each of which internal forces and reaction forces are derived. The actions and their respective stresses are then superpositioned to produce the overall internal stress and reactions from the load heterodyne.

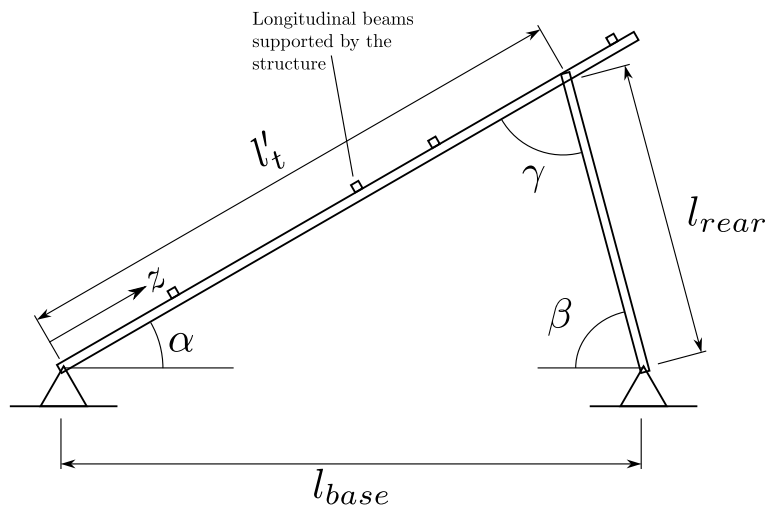


Figure 3.13.: Measurements and notations of the substructure

Reaction forces from elementary load cases

Perpendicular load on transversal beam: Moment equilibrium with front support as centre of rotation gives the rear vertical reaction:

$$\curvearrowright \quad R_{rear,v} = \sum P_{\perp,k} \cdot z_k \frac{1}{l_{base}} \quad (3.23)$$

3. Loads and statics

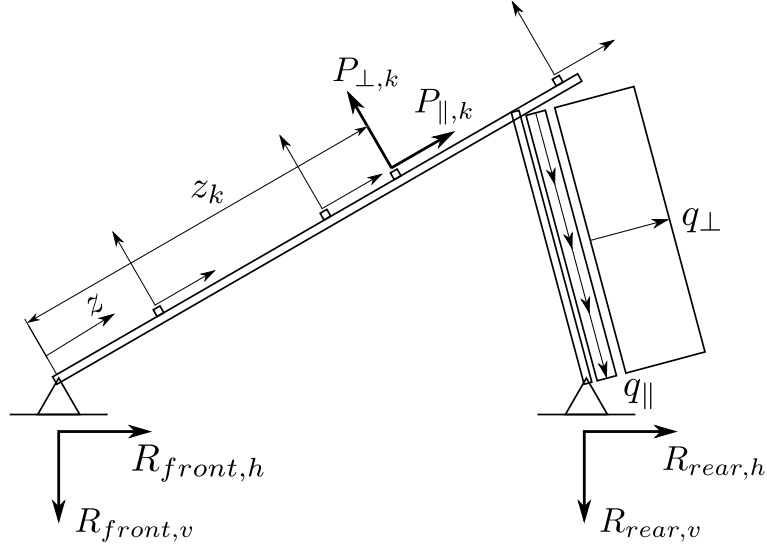


Figure 3.14.: Loads and reactions acting on the triangular substructure

Vertical equilibrium:

$$(\uparrow) \quad R_{\text{front},v} = \sum P_{\perp,k} \cdot \cos(\alpha) - R_{\text{rear},v} \quad (3.24)$$

Perpendicular load on transversal beam causes a normal force in the rear element:

$$\begin{aligned} N_{\text{rear}} &= \frac{\sum P_{\perp,k} \cdot z_k}{l'_t \cdot \sin(\gamma)} \\ R_{\text{rear},h} &= -N_{\text{rear}} \cdot \cos(\beta) \end{aligned} \quad (3.25)$$

Horizontal equilibrium:

$$R_{\text{front},h} = - \left(\sum P_{\perp,k} \cdot \sin \alpha + R_{\text{rear},h} \right) \quad (3.26)$$

Parallel load on transversal beam: Constructing the moment equilibrium around the front support hinge shows that this load case causes no reaction at the rear support, since the lever arm with respect to the front support is zero for all loads. Thus:

$$R_{\text{rear},v} = 0 \quad (3.27)$$

$$R_{\text{rear},h} = 0 \quad (3.28)$$

Thus, all loads must be transferred through the front support:

$$R_{\text{front},v} = \sum_k P_{\parallel,k} \cdot \sin(\alpha) \quad (3.29)$$

$$R_{\text{front},h} = \sum_k P_{\parallel,k} \cdot \cos(\alpha) \quad (3.30)$$

$$(3.31)$$

Perpendicular load on rear beam: Moment equilibrium with rear support as centre of rotation gives the front vertical reaction:

$$\curvearrowleft \quad R_{\text{front},v} = \frac{q_{\perp} \cdot l_{\text{rear}}^2}{2l_{\text{base}}} \quad (3.32)$$

Vertical equilibrium:

$$(\uparrow) \quad R_{\text{rear},v} = q_{\perp} \cdot l_{\text{rear}} \cdot \cos(\beta) - R_{\text{front},v} \quad (3.33)$$

Normal force in transversal beam causes a horizontal reaction at the front:

$$R_{\text{front},h} = \frac{q_k \cdot l_{\text{rear}}}{2 \sin \gamma \cdot \cos \alpha} \quad (3.34)$$

Horizontal equilibrium:

$$R_{\text{rear},h} = \frac{q_k \cdot l_{\text{rear}}}{\sin \beta} - R_{\text{front},h} \quad (3.35)$$

Parallel load on rear beam: Since the parallel load acting on the rear beam likewise posses no lever arm with respect to the rear support, all of the action is lead into the rear support:

$$P_{\text{rear}} = q_{\parallel} \cdot l_{\text{rear}}$$

$$R_{\text{rear},v} = P_{\text{rear}} \cdot \sin(\beta) \quad (3.36)$$

$$R_{\text{rear},h} = P_{\text{rear}} \cdot \cos(\beta) \quad (3.37)$$

Thus, no loads can be transferred through the front support:

$$R_{\text{front},v} = 0 \quad (3.38)$$

$$R_{\text{front},h} = 0 \quad (3.39)$$

Internal forces from elementary load cases

The internal forces are determined by creating free body diagrams of the structural elements with their respective loads, reactions and forces from adjoining elements.

3. Loads and statics

Transversal beam Bending moments are derived by, once again, superpositioning the internal stress from the single loads acting on the structure. Two base cases are recognized. When the load is placed above the upper support, the bending moment is given by:

$$z \leq l'_t \quad : \quad M_{\text{front}}(z) = P_{\perp,k}(z_{P,k} - l'_t) \frac{z}{l'_t} \quad (3.40)$$

$$l'_t < z \leq z_{P,k} \quad : \quad M_{\text{front}}(z) = P_{\perp,k}(z_{P,k} - z) \quad (3.41)$$

$$z_{P,k} < z \quad : \quad M_{\text{front}}(z) = 0 \quad (3.42)$$

When the concentrated load acts between the supports:

$$z \leq z_{P,k} \quad : \quad M_{\text{front}}(z) = P_{\perp,k}(l'_t - z_{P,k}) \frac{z}{l'_t} \quad (3.43)$$

$$z_{P,k} < z \leq l'_t \quad : \quad M_{\text{front}}(z) = P_{\perp,k} \cdot z_{P,k} \frac{(l'_t - z)}{l'_t} \quad (3.44)$$

$$l'_t < z \quad : \quad M_{\text{front}}(z) = 0 \quad (3.45)$$

Again, by adding up the bending moments for all cases, the moment distribution of the transversal beam is determined.

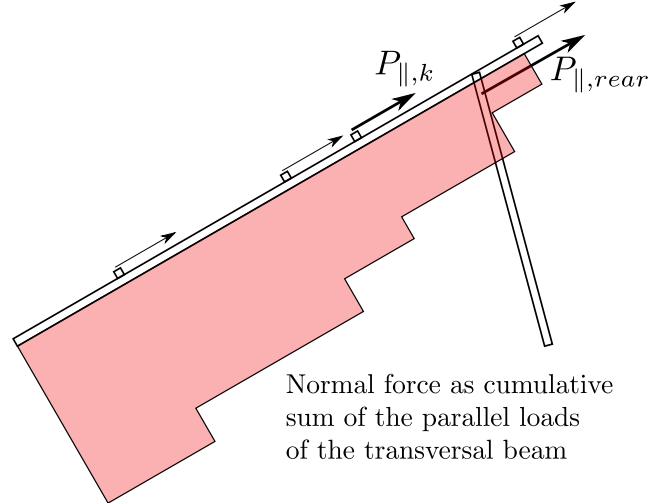


Figure 3.15.: Accumulative normal force of the transversal beam

Normal forces of the transversal beam are derived by cumulatively adding the actions parallel to the beam, from its rear end down to the front support of the frame, finding the largest value (this principle is shown in Figure 3.15). The parallel reaction from the rear

beam is determined through:

$$\begin{aligned} P_{\parallel, \text{rear}} &= q_{\perp} \frac{l_{\text{rear}}}{2 \sin(\gamma)} \\ N_{\text{front}} &= \max \left[\sum P_{\parallel} \right] \end{aligned} \quad (3.46)$$

Rear beam The **bending moment** of the rear beam is simply determined, since this part only have one transversal load:

$$M_{\text{rear}} = q_{\perp} \cdot \frac{l_{\text{rear}}^2}{8} \quad (3.47)$$

The **normal force** is derived by transforming reaction forces from the rear support into their parallel components of the beam. This has to be done separately for cases where the beam works as a truss beam (no transversal loads) and for the case of transversal load:

$$N_{\text{rear}} = R_{q_{\perp}, v} \sin(\beta) - R_{q_{\perp}, h} \cos(\beta) + \frac{R_{q_{\parallel}, v} + R_{P_{\perp}, v}}{\sin(\beta)} \quad (3.48)$$

4. Wind actions for varying geometries

This chapter constitutes the main part of this study, where results from different wind tunnel experiments (kindly provided by wind tunnel operators in Germany) are compared to the NVN 7250 pre-standard.

4.1. Standard case according to the NVN 7250

In this section, the approach to wind loads and to determining the ballast quantities described in the NVN 7250 follows. An example application of the method is also given.

4.1.1. Building and mounting system geometry of the base case

The mounting system and building geometry presented here is used throughout this chapter.

Mounting system

The type of mounting systems considered in this thesis are called “mounting system type 3” (flat roof, module elevated and inclined) in the NVN 7250 pre-standard. The mounting systems are subclassed according to module inclination:

1. Inclination less than 10 degrees.
2. Inclination between 10 and 40 degrees.
3. Inclination between 40 and 70 degrees.

For this description, the focus lies on the 2nd category, since the optimal module inclination is 30 degrees for northern Europe (Erfurth, 2001). Further, this category is divided into *open* and *closed* structures (see Section 2.1.1 and 2.1.3, respectively). A *closed* structure is defined as one where *all* visible faces are closed or screened off from wind; front, rear and cross-cut sides (“gables”).

Building geometry and module layout

The NVN 7250 assumes a flat-roofed, rectangular building (Section 5.1.1.4.2), with a slope smaller than 10 degrees and without interrupting building installations. The roof is divided into *corner*, *edge* and *middle* zones, according to the existing Dutch wind load standard *NEN 6702*. A fourth zone, *rooftop structure* (Dutch: *dakopbouw*), is given for buildings with varying roof heights. This division is done using Figure 4.1 and Equations (4.1)–(4.3).

4. Wind actions for varying geometries

$$a = \begin{cases} 0.15d_1 \geq 1.0 \text{ m} & d_1 \leq 3h \\ 0.45h \geq 0.04d_1 \geq 1.0 \text{ m} & d_1 \geq 3h \end{cases} \quad (4.1)$$

$$a_1 = \begin{cases} a & d_2 \geq 1.5d_1 \\ 0.5d_1 \left(1.5 - \frac{d_2}{d_1}\right) + a \left(\frac{d_2}{d_1} - 0.5\right) & d_2 < 1.5d_1 \end{cases} \quad (4.2)$$

$$a_2 = \begin{cases} 0.5d_1 & d_2 \geq 1.5d_1 \\ 0.5d_1 \left(\frac{d_2}{d_1} - 0.5\right) + a \left(1.5 - \frac{d_2}{d_1}\right) & d_2 < 1.5d_1 \end{cases} \quad (4.3)$$

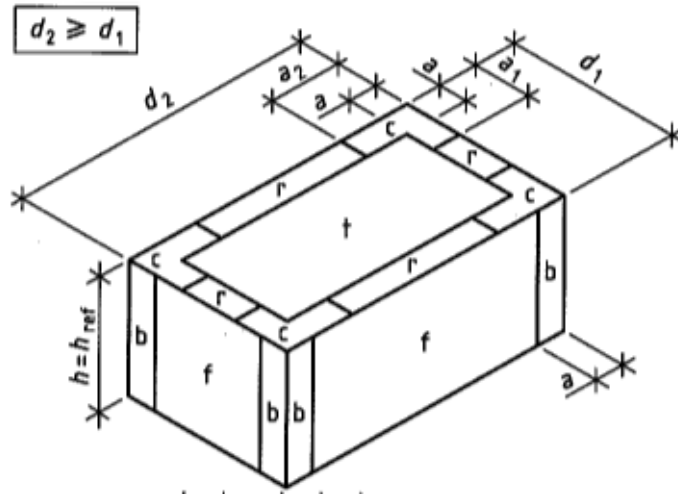


Figure 4.1.: The load zones of a flat roof (Nederlands Normalisatie-instituut, 2007, chap. A.2)

The modules are assigned wind load coefficients according to the following parameters:

- Load zone on the roof
- Open or closed supporting structure
- Separate values are given for roofs with *parapets* > 200 mm. The values can be linearly interpolated for shorter parapets $100 < h < 200$ mm.

The modules are assumed to be laid out in straight, evenly spaced rows, parallel to one of the building's main axes. While this is not explicitly stated in the Dutch pre-standard, the foregoing studies (Geurts and van Bentum, 2007; Geurts, Ravenhorst, and Donkervoort, 2002), were conducted without parameterizing neither module angle in the horizontal plane (relative to eaves) nor module spacing (see Section 2.3.2). It is therefore safer to restrict the standard case discussed here to evenly spaced and parallel modules.

4.1.2. Wind action model of the NVN 7250

The actions on the structures are derived in Section 3.1.1. The heterodynes 3–5 from this section are used for dimensioning the steel structure, which is not shown in this section. The necessary ballast to keep the structures in place is derived below in Section 4.1.3 using a load combination specific to the NVN 7250.

The dynamic wind pressure is derived using the roof height as reference height, and the varying loads on the solar panels are expressed through the wind load coefficients shown in Table 4.1, where loads are assumed to be constant over the module surface.

Table 4.1.: Wind load coefficients for different roof areas, for roofs without parapets (Netherlands Normalisatie-instituut, 2007, Table 4).

Roof zone	c_p , upwards	c_p , downwards
c (corner)	-1.8	1.2
r (edge)	-1.6	1.2
p (latern)	-1.6	1.2
t (center)	-0.6	0.6
t (center, protected)	-0.4	0.4

Assigning load zones to modules

The load zones need to be simplified to fit into the load model described in Section 3.1.1. Two edge cases for the intersections between load zones and modules need to be normalized to fit the static model, where borders between load zones are assumed to be perpendicular to the long axis of the mounting system (see Section 3.1.1).

1. When zone borders are not perpendicular to the modules (Figure 4.2), the furthest corner of the zone with larger load takes precedence.
2. When two zones run parallel along the longitudinal axis of the mounting system, precedence is given to the zone with larger load (see Figure 4.3).

4.1.3. Ballast quantity derivation according to NVN 7250

The necessary amount of ballast is to be determined through the method shown in the normative Appendix B of the NVN 7250. There are two failure mechanisms to be investigated, **tipping** and **horizontal displacement**. Only wind forces and dead load is applied when determining the needed ballast quantity in the load combination shown in Eq. 4.4.

$$0.9 \cdot (G_{\text{Frame}} + G_{\text{Panel}} + G_{\text{Ballast}}) - 1.3 \cdot F_{\text{Wind}} = 0 \quad (4.4)$$

4. Wind actions for varying geometries

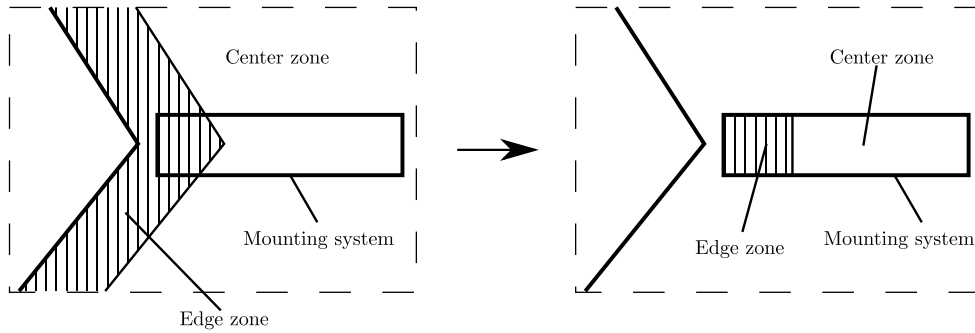


Figure 4.2.: Load zone borders oblique to module edges

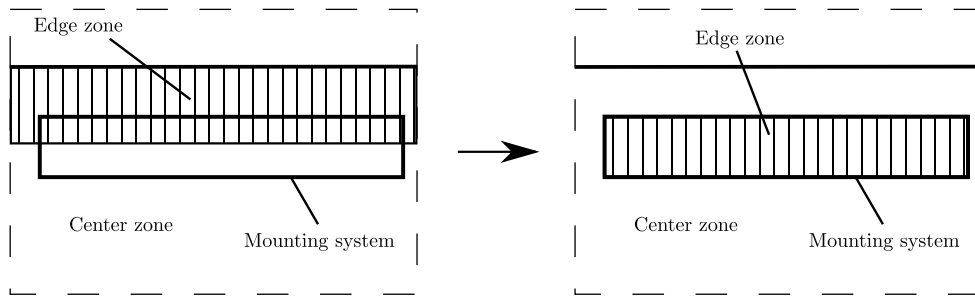


Figure 4.3.: Load zones varying across the modules

That is, favorable actions are reduced and unfavorable actions (causing uplift and displacement) are increased.

Tipping or tilting

Tipping is treated differently for open and closed mounting systems. For open systems, the wind pressure is summed up into a concentrated load, acting on three-quarters of the width of the module surface (see Figure 4.4). For the closed structure, the resulting forces on both the front and rear surface are located in the middle of the respective surface (Figure 4.5). The structure needs to be in static equilibrium when the ballast and its placement relative to the front support is accounted for. The following condition needs to be fulfilled to secure the structure against tipping:

$$0 = 1.3 \cdot M_W - 0.9 \cdot (M_G + M_B) \quad (4.5)$$

4.1. Standard case according to the NVN 7250

where

$$M_W = b_{panel} \cdot q_w \cdot L_{wind}$$

$$M_G = b_{panel} \cdot g_{panel} \cdot \frac{b_{panel}}{2} \cos \alpha$$

$$M_B = L_{ballast} \cdot G_{ballast, rear}$$

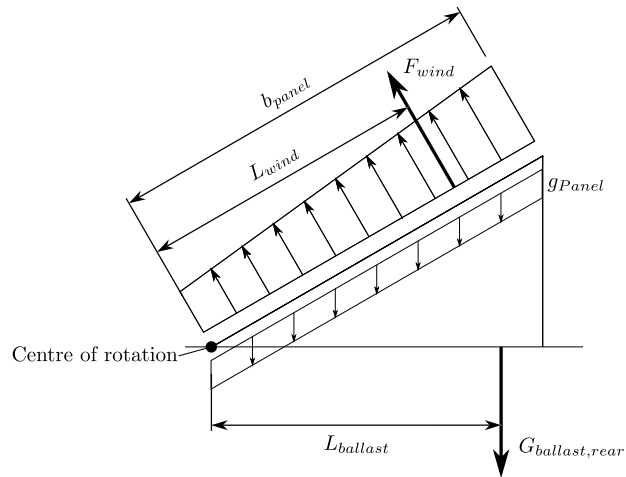


Figure 4.4.: Illustration of failure mode "tipping", open structure

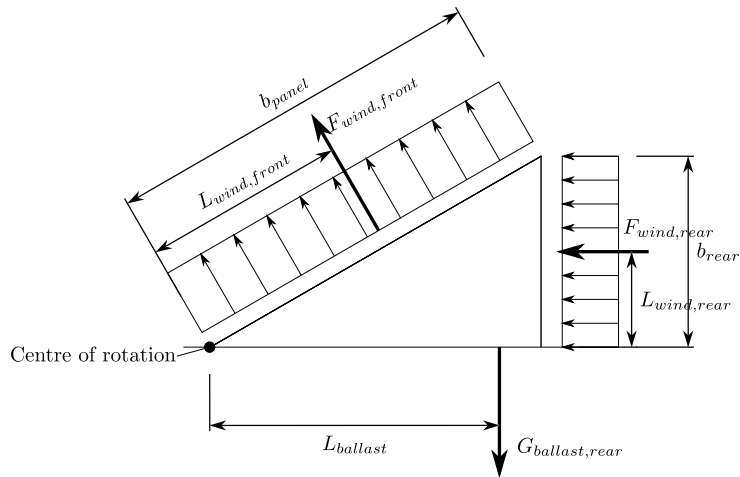


Figure 4.5.: Illustration of failure mode "tipping", closed structure

4. Wind actions for varying geometries

Horizontal displacement

Using the same loading approach as in the previous paragraph, the resulting horizontal actions on the structure must be surpassed by the friction force capacity from the resulting downwards forces. The friction force capacity is determined with Eqn. 4.6, using the static friction coefficient μ to determine the friction between support and roofing. The coefficient of friction can be assumed as $\mu = 0.5$ (Lieb, 2009, p. 7).

$$F_{\text{Friction}} = \mu \cdot \sum F_{\text{Vertical}} \geq F_{\text{Horizontal}} \quad (4.6)$$

where

$$F_{\text{Vertical}} = 0.9 \cdot (G_{\text{Frame}} + G_{\text{Panel}} + G_{\text{Ballast,front}} + G_{\text{Ballast,rear}}) - 1.3 \cdot F_{\text{Wind}} \cdot \cos \alpha$$

and

$$F_{\text{Horizontal}} = 1.3 \cdot F_{\text{Wind}} \cdot \sin \alpha$$

As in the tipping equilibrium, the resulting downwards force, as well as the horizontal force from wind pressure, is determined with the weighting from Equation 4.4.

Gently pitched roofs

Placing the mounting system on a pitched surface, causes the dead loads to get components parallel to the roof surface, which in its turn increases the horizontally displacing forces. Therefore, the ballast weight needed to keep the mounting system in place through friction also increases (see Figure 4.6).

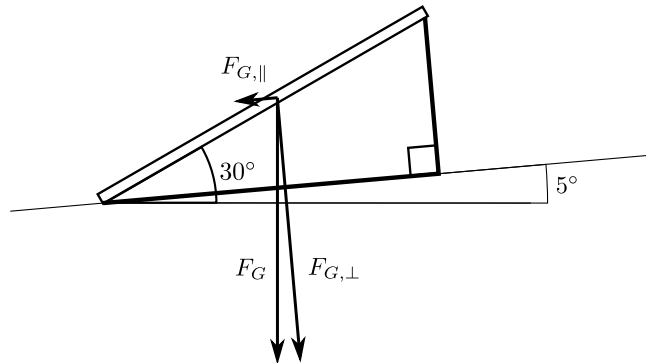


Figure 4.6.: Roof-parallel components of dead loads on inclined roofs

4.1.4. Usage example

Wind loads and ballast are determined for roof-mounted photovoltaic modules within the constraints given in Section 4.1.1, to illustrate the procedure. It is shown how the ballast is determined for a single mounting system, and the assigned wind load coefficients and resulting ballast amounts are illustrated for the entire arrangement.

Load assumptions

For the sake of simplicity, the dynamic wind pressure on the reference height z_e of the building is assumed to be $q_k = 1.0 \text{ kN/m}^2$ and the dead weight of the solar collectors $g_k = 0.2 \text{ kN/m}^2$. The snow load is neglected completely, since it is a non-permanent, favorable action when determining the necessary ballast amount, (see Section 3.1.1).

Building geometry and module layout

The building considered for this example measurements $23 \times 30 \text{ m}$, with a height of 10 m. A top view of the roof with the module layout is shown in Figure 4.7. The mounting systems, of the “open” kind without rear surface for uplift reduction (see Section 2.1.1), have a projected width of 1 m, and a lateral spacing of 1.5 m. Along the edges of the roof, a 1 m wide border is left free of modules, which means that each module row is 28 m wide, with supporting frames symmetrically arranged each 1.5 m. The measurements of the mounting systems are shown in Figure 4.8.

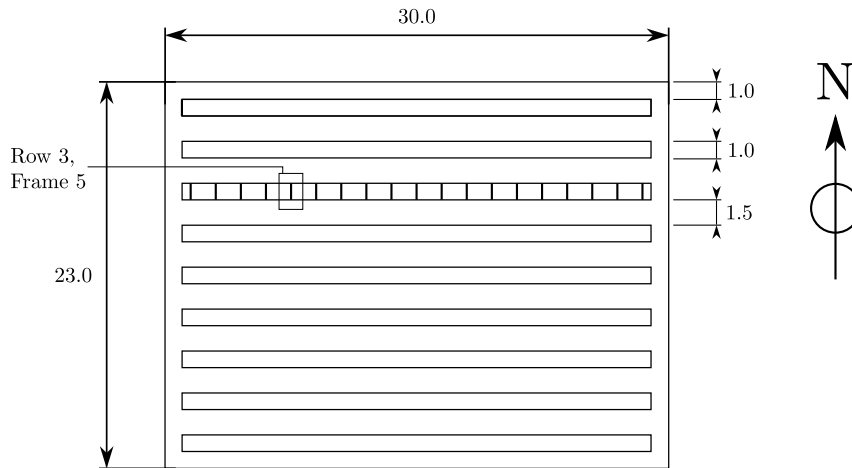


Figure 4.7.: Illustration of roof geometry and module layout.

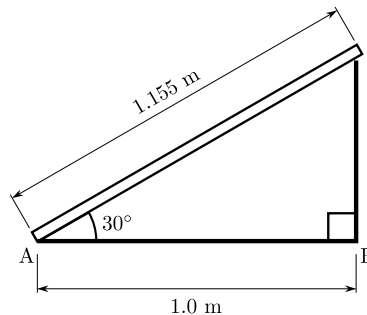


Figure 4.8.: Illustration of mounting system measurements.

4. Wind actions for varying geometries

Determining wind pressure coefficients.

The roof is divided into load zones as described in Section 4.1.1, with the result shown in Figure 4.9a, along with the prescribed wind pressure coefficients. The resulting load zone assignment for each mounting system is shown in Figure 4.9b. Three different set of load zones intersecting the modules are identified: Edge rows, with *corner* and *edge* zone loads acting on them, the rows behind them, and center rows, intersecting with the *edge* and *center* zones.

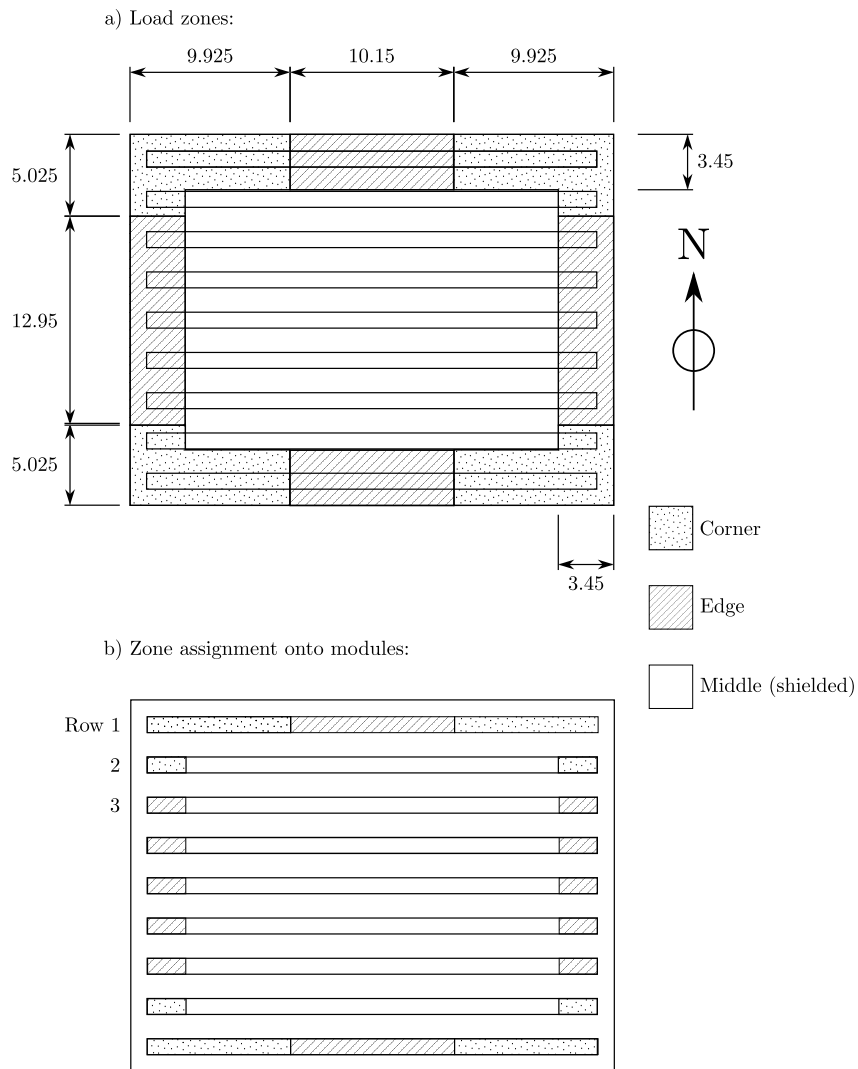


Figure 4.9.: Resulting division of the roof into different load zones (above) and resulting assignment (below).

Ballast

In order to factor in the off-centre wind force described in Section 4.1.3, the wind load and dead load need to be treated separately. The ballast derivation is shown here for *row 3, frame 5*, for which the location is shown in Figure 4.7.

The load acting on the frame considered is determined using the longitudinal beam statics from Section 3.2.1. By applying the wind and dead loads separately to a longitudinal beam system equivalent to the module surface as a beam, with the frames as supports, the distributed wind and dead loads can be reduced to line loads $q_{w,line}$ and $g_{panel,line}$ acting on the frame.

$$\begin{aligned} q_{w,line} &= 0.60 \text{ kN/m} \\ g_{panel,line} &= 0.30 \text{ kN/m} \end{aligned}$$

The amount of ballast at the front and rear support of the specific frame are then derived by solving Equations for *tipping* (4.5) and *horizontal displacement* (4.6):

$$\begin{aligned} 0 &= M_W \cdot 1.3 - 0.9 \cdot (M_G + M_B) \iff \\ G_{ballast,rear} &= \frac{1}{b_{panel} \cos \alpha} \left(M_W \cdot \frac{1.3}{0.9} - M_G \right) \\ &= \frac{1}{1.155 \cos 30^\circ} \left(0.60 \cdot \frac{1.3}{0.9} - 0.173 \right) \\ &= 0.70 \text{ kN} \end{aligned}$$

Rearranging (4.6) determines the ballast on the front support:

$$\begin{aligned} G_{ballast,front} &= F_{Wind} \frac{1.3}{0.9} \left(\frac{\sin \alpha}{\mu} + \cos \alpha \right) - G_{Frame} - G_{Panel} - G_{Ballast, rear} \\ &= \frac{1.3}{0.9} \cdot q_{w,line} b_{panel} \left(\frac{\sin 30^\circ}{0.5} + \cos 30^\circ \right) - 0 - b_p \cdot g_{panel,line} - 0.7 \text{ kN} \\ &= \frac{1.3}{0.9} \cdot 0.7 \left(\frac{0.5}{0.5} + \frac{\sqrt{3}}{2} \right) - 0 - 0.3 \cdot 1.155 - 0.7 \\ &= 0.84 \text{ kN} \end{aligned}$$

Note that mounting system is assumed to be weightless ($G_{Frame} = 0$). The weight of the mounting system can otherwise be subtracted from the overall ballast quantity. Similar calculations are performed for each frame of each mounting system. The resulting loads are shown in Table 4.2. Since only three different load zone configurations on the modules are identified, the ballast is only shown for each of these configurations.

The distribution of the ballast is also shown in the diagram in Figure 4.10. The ballast quantity needed seems more or less constant along the edges of the building, whereas it clearly decreases in the center, shielded region of the roof.

4. Wind actions for varying geometries

Table 4.2.: Resulting ballast amounts (kN) for each frame and support on the example layout. Rows 1–3 refers to Figure 4.9.

	Row 1			Row 2			Row 3		
	Zone	Front	Rear	Zone	Front	Rear	Zone	Front	Rear
Support 1	Corner	3.46	2.98	Corner	3.54	3.05	Edge	3.13	2.69
Support 2		4.52	3.89		3.80	3.27		3.38	2.91
Support 3		4.28	3.68		0.69	0.58		0.71	0.59
Support 4		4.34	3.74		0.87	0.73		0.86	0.72
Support 5		4.33	3.73		0.82	0.68		0.82	0.69
Support 6		4.33	3.72		0.83	0.70		0.83	0.70
Support 7		3.91	3.36		0.83	0.69		0.83	0.69
Support 8		3.82	3.28		0.83	0.69		0.83	0.69
Support 9	Edge	3.84	3.30	Center	0.83	0.69	Center	0.83	0.69
Support 10		3.83	3.29		0.83	0.69		0.83	0.69
Support 11		3.84	3.30		0.83	0.69		0.83	0.69
Support 12		3.82	3.28		0.83	0.69		0.83	0.69
Support 13		3.91	3.36		0.83	0.69		0.83	0.69
Support 14		4.33	3.72		0.83	0.70		0.83	0.70
Support 15		4.33	3.73		0.82	0.68		0.82	0.69
Support 16	Corner	4.34	3.74		0.87	0.73		0.86	0.72
Support 17		4.28	3.68		0.69	0.58		0.71	0.59
Support 18		4.52	3.89	Corner	3.80	3.27	Edge	3.38	2.91
Support 19	3.46	2.98	3.54		3.05	3.13		2.69	

The ballast quantity derived here isn't very practical for assembly reasons: Different concrete blocks have to be ordered and assigned to the right positions on the roof. It would be desirable to get the different weights at each support down to one or two types.

4.1.5. Adaption for real-world usage

The roof load zones and load heterodyne used to determine the ballast quantity in this section (4.1.1 and 4.1.3, respectively) are retrieved from the NVN 7250, since they are part of the actual, suggested dimensioning method. To adapt the dimensioning to the Eurocode (EN-1991-1-4 and EN 1990), these parts need to be replaced with their Eurocode equivalents.

As stated above, the ballast need to be distributed more evenly on the roof surface. The first measure would be to distribute the weight evenly between the front and rear support of each frame. However, the uplift forces also varies wildly between edge or corner areas and center areas. Placing the largest weights needed at every support would clearly be uneconomical and probably render the module arrangement unfeasible (Ruscheweyh and

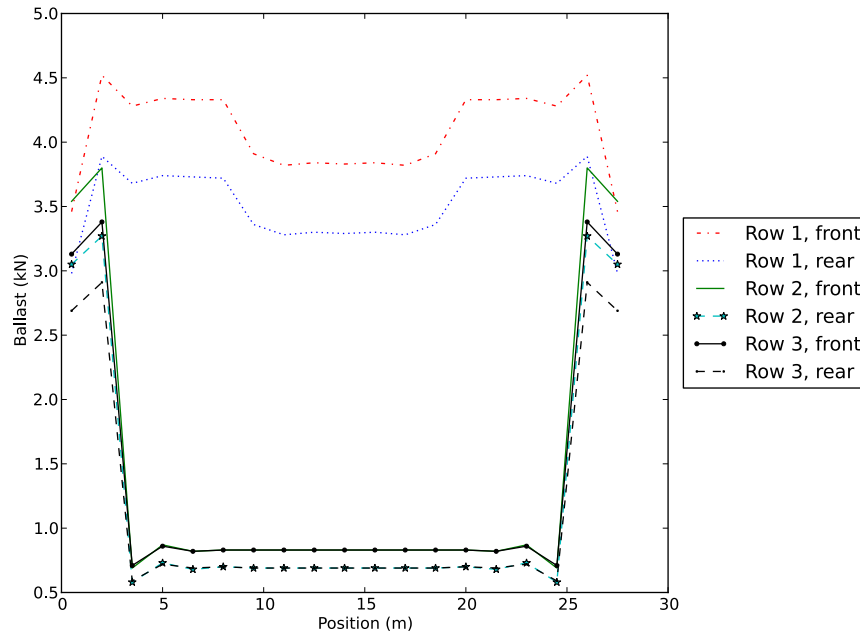


Figure 4.10.: Representation of the variation in needed ballast along different lines of the roof.

Windhövel, 2009).

In the example above, imagine the outer rows (“row 1”) as being treated separately from the inner (“row 2–3”), since the ballast quantity for the outer rows are determined to be much larger. One possibility would be to distribute the total ballast quantity evenly among the supports. Such a distribution is however also not realistic, since the outer supports may lift from the roof and cause an internal failure of the mounting system. A different suggestion would be to separate the modules into “heavy” (corner and edge areas) and “light” (center of the roof) mounting systems, where the all structures in each group would have ballast equal to the largest uplift force encountered in the group attached. Of course, the adaption of the ballast quantity results to real world constraints must be done on a case-to-case-basis.

4.2. Modules oblique to building walls

When one of the principal axes of a rectangular building isn’t going in a north-south direction, the modules will be oblique towards the walls. This variable wasn’t investigated in the studies preceding the NVN 7250 (see Section 2.3.2). A comparison is therefore being made between results published by Ruscheweyh and Windhövel (2005), *Windlasten an*

4. Wind actions for varying geometries

großflächig angeordneten Photovoltaik-elementen (Wind actions on larger arrays of photovoltaic elements, author's translation), and a suggested approach to determine the wind actions using the NVN 7250.

4.2.1. Building and mounting system geometry

The study by (Ruscheweyh and Windhövel, 2005) investigates wind loads on photovoltaic panels on a complex of industrial halls. Investigations were made for two smaller parts of the hall, to investigate uplift forces and downwards forces, respectively. Only the part of the building investigated for uplift forces is considered in this section.

Mounting system geometry

The mounting system and module geometry for this example is shown in Figure 4.11. The module has the dimensions 1.708×0.79 m, and an inclination of 25 degrees. The gap between the module eave and the roofing is 0.3 m. The NVN 7250 does not factor in possible influence on the wind action from this gap, while it is implicitly considered in the case study by Ruscheweyh and Windhövel, since it is part of the actual investigated geometry. The distance between the supports on each frame is assumed to be 0.79 m.

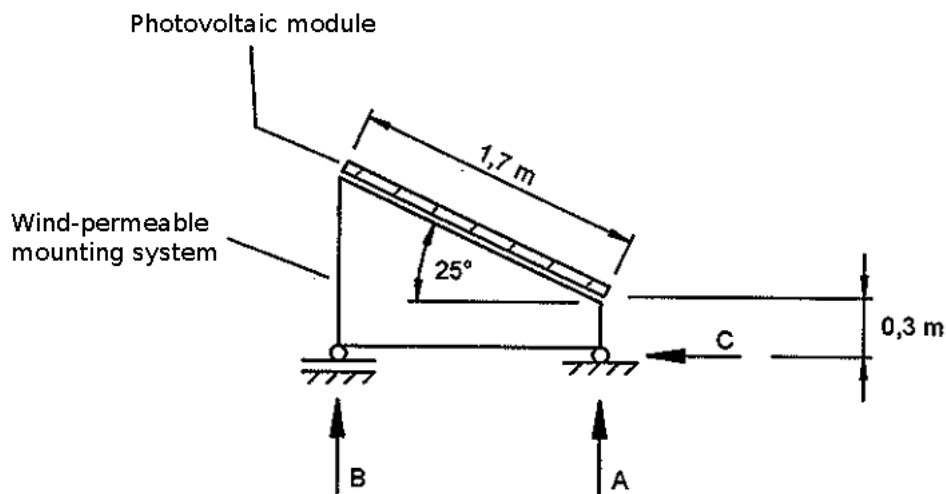


Figure 4.11.: Schematic section of the mounting system (Ruscheweyh and Windhövel, 2005).

Building geometry

The hall complex concerned here consists of four halls, shown in Figure 4.12 with the part being investigated (Hall 2) for uplift forces highlighted by the author. A rough outline of

the module arrangement can also be seen. The angle between the hall complex' principal axis and the north axis is 30 degrees. The roof height of the hall is overall 10 m.

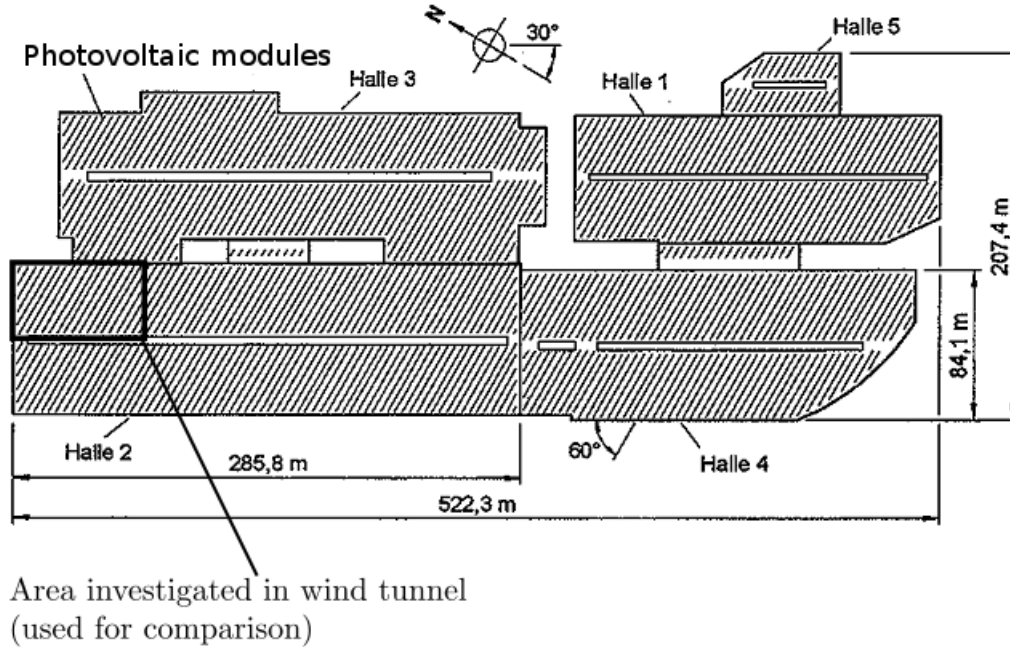


Figure 4.12.: Top view of the industrial hall complex (Ruscheweyh and Windhövel, 2005, modifications by author)

4.2.2. Wind action model according to Ruscheweyh and Windhövel

The roof is divided into 8 different load zones, with borders parallel to the panel rows (Figure 4.13). The zones corresponds to wind actions described by the coefficients shown in Figure 4.14, except for zone **h** which equals zone **g** multiplied with a factor $\psi = 0.6$.

The wind-induced pressure described by Figure 4.14 vary across the module surface on the most exposed parts of the roof. Horizontal forces, F_x , and uplift, F_z , are derived from the horizontal and vertical components of the wind pressure. A third force, F_y , acting in the longitudinal direction of the mounting system, is also described in the report as:

$$F_y = c_r \cdot A_r \cdot q_b \cdot \psi \quad (4.7)$$

where

$$\begin{aligned} \psi_{friction} &= \text{Reduction factor from wind direction and shadowing effects} \\ c_r &= \text{Friction coefficient} = 0.02 \end{aligned} \quad (4.8)$$

4. Wind actions for varying geometries

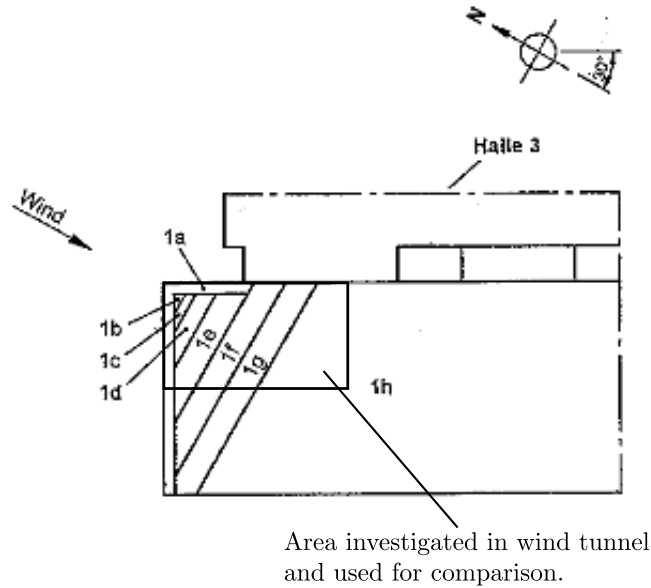


Figure 4.13.: Load zones on the roof of hall 2 (Ruscheweyh and Windhövel, 2005).

Ruscheweyh and Windhövel do not provide values for $\psi_{friction}$ in this report. Equation (4.7) implies that the largest horizontal force induced by friction between wind and module surface is at most $F_y = 0.02 \text{ kN/m}^2$ for a dynamic wind pressure of $q_w = 1.0 \text{ kN/m}^2$, which is neglected when determining the ballast quantities in the subsequent calculations. The effect from wind friction, however, has to be regarded when calculating the impact from additional wind actions on the bracing of the supporting building (Ruscheweyh and Windhövel, 2005).

The approach suggested here includes transient loads, to be applied on $5 \times 5 \text{ m}$ areas at a time, using the coefficients shown in Figure 4.15. In this case, only the coefficients on the left are used, since they represent the largest uplift forces. For this application, the transient load case is applied to a 5 m length of each row at a time.

4.2.3. Ballast quantity derivation according to Ruscheweyh and Windhövel

Since the wind action is not uniformly distributed across the panel surface (Figure 4.14), the excentric point of action of the resulting wind force suggested by Section 4.1.3 is implied by the increased wind action on the upper part of the modules. The method of condensing distributed loads into line loads acting on each frame, to derive this resulting load, is therefore not relevant. Instead, the resulting action on the frame exerted by the longitudinal beams are derived, and the wind-induced support reactions are derived from the static equilibrium of the frame, which is illustrated in Figure 4.16.

Similarly to the ballast model described in section 4.1.3, dead load and wind actions are treated separately, to be able to weigh the friction from dead load minus uplift when

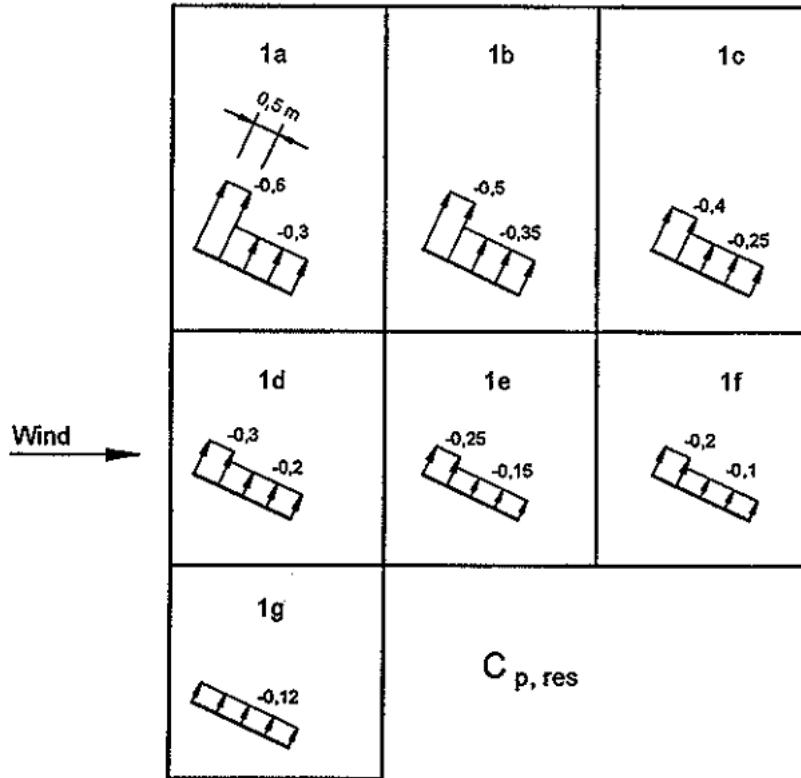


Figure 4.14.: Wind uplift coefficients corresponding to roof areas in Figure 4.13 (Ruscheweyh and Windhövel, 2005).

countering friction loads. The partial factors γ_{Wind} and γ_G used here are the same as in Section 4.1.3. The ballast is assumed to be located at the respective supports, making the lever for the rear ballast $L_{ballast}$ equal to the projected width of the mounting system L_{base} .

for **tipping**:

$$G_{ballast,rear} = \frac{\gamma_{Wind} R_{v,rear} \cdot L_{base}}{\gamma_G L_{ballast}} \geq 0 \quad (4.9)$$

for **horizontal displacement**:

$$\begin{aligned} F_h &= \frac{\gamma_{wind} (R_{h,front} + R_{h,rear})}{\mu} \\ F_v &= \gamma_{Wind} (R_{v,front} + R_{v,rear}) \\ G_{ballast,front} &= \frac{F_h + F_v}{\gamma_G} - G_{ballast,rear} \end{aligned} \quad (4.10)$$

4. Wind actions for varying geometries

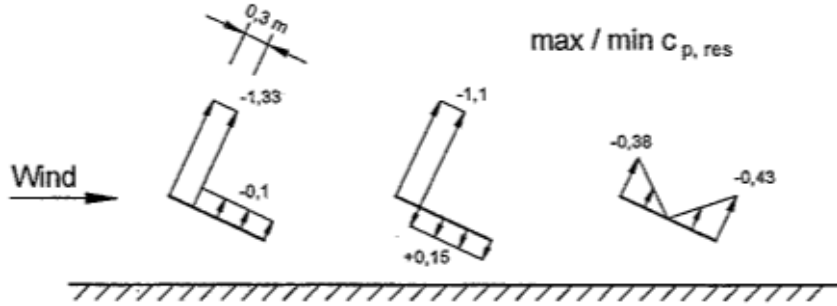


Figure 4.15.: Pressure coefficients for transient loads (Ruscheweyh and Windhövel, 2005)

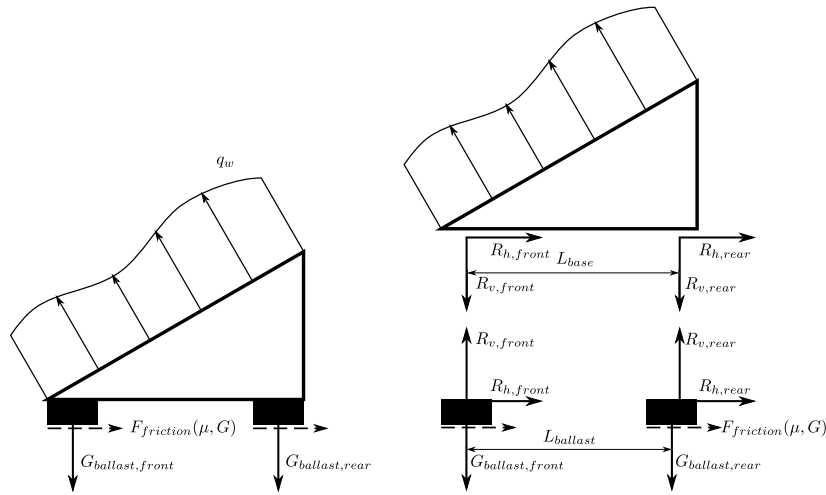


Figure 4.16.: Outer (left) and inner (right) static equilibrium between wind forces, support reactions and ballast.

if $G_{ballast,front} \geq G_{ballast,rear}$, balance the weight between front and rear support:

$$G'_{ballast,front} = G'_{ballast,rear} = \frac{G_{ballast,front} + G_{ballast,rear}}{2} \quad (4.11)$$

Global equilibrium of structure

The transient loads described in section 4.2.2 are applied to 5-meter intervals of each row. When considering loss of static equilibrium (EQU) for the entire structure, the most dangerous situations occur when the transient loads are applied to the ends of the structure (see Figure 4.17), causing uplift on one end. By deriving the necessary ballast quantities for these actions, assuming a constant ballast distribution, the mounting system will be able to maintain static equilibrium no matter where the transient load is applied (placing the transient load closer to the pivot point induces a smaller moment M_{uplift} around the pivot point **A**). Further, since the largest wind actions occur at the ends of the structure

(e.g. Figure 4.9), the transient load is also placed mid-structure, which induces the largest total uplift and horizontal forces. For this to work, the structure is assumed to remain rigid and to be able to redistribute the support reactions among the transversal frame, an assumption supported by the reports from Ruscheweyh and Windhövel in this study, esp. Ruscheweyh and Windhövel (2005) and also Lieb (2009, p. 5).

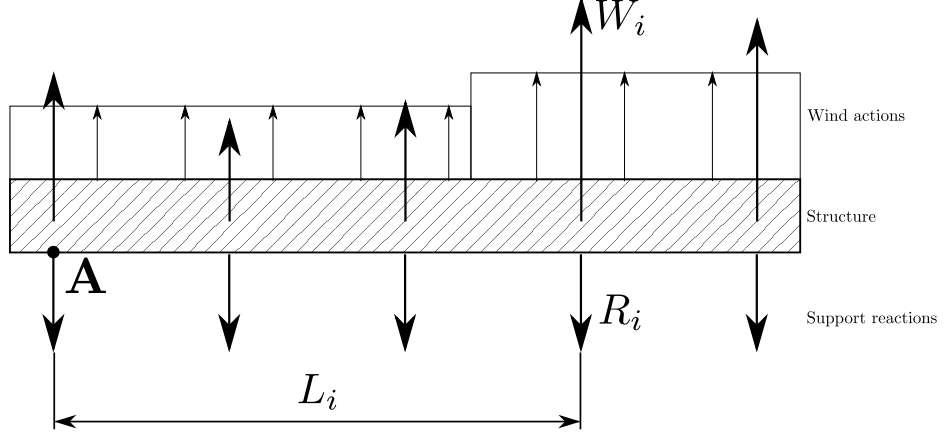


Figure 4.17.: Loss of static equilibrium for entire mounting system caused by transient wind action.

The ballast quantities required when applying the transient loads are derived using moment equilibriums with the pivot point at the support farthest from the area where the transient load is applied (see Figure 4.17).

$$M_{uplift,A} = \gamma_W \cdot \sum_i W_{v,i} \cdot L_i$$

$$M_{ballast,A} = \gamma_G \cdot \sum_i R_i \cdot L_i$$

Assuming R_i is constant and the condition for EQU, $M_{uplift,A} = M_{ballast,A}$:

$$R_i = \frac{\sum_i W_{v,i} \cdot L_i \cdot \gamma_W}{\sum_i L_i \cdot \gamma_G} \quad (4.12)$$

To solve the static equilibrium for horizontal forces, again choosing one of the outer supports as pivot point, the uplift forces need to be subtracted from the weight placed at each support:

$$M_{horizontal,A} = \gamma_W \cdot \sum_i W_{h,i} \cdot L_i$$

$$M_{friction,A} = \sum_i (\gamma_G R_i - \gamma_W W_{v,i}) L_i \mu$$

4. Wind actions for varying geometries

Once again, assuming constant ballast distribution:

$$R_i = \frac{1}{\gamma_G \sum_i L_i} \gamma_W \sum_i \left(\frac{W_{h,i}}{\mu} + W_{v,i} \right) L_i \quad (4.13)$$

For vertical and horizontal equilibrium, the following expressions are used (assuming N supports):

$$R_{i,vert} = \frac{\gamma_W}{\gamma_G} \cdot \frac{\sum_{i=1}^N R_{v,i}}{N} \quad (4.14)$$

$$R_{i,horizontal} = \frac{\gamma_W}{\gamma_G \cdot N} \sum_{i=1}^N \left(\frac{R_{h,i}}{\mu} + R_{v,i} \right) \quad (4.15)$$

Choosing the ballast quantities at each support yielded by the different derivation approaches (Eqn. (4.11), (4.12), (4.13), (4.14), (4.15)), the final ballast quantity is derived.

4.2.4. Application - Ruscheweyh and Windhövel

The wind actions and ballast quantities necessary for static equilibrium are derived for a simple module layout, namely the one used in the wind tunnel investigation. For the comparison, only the part of Hall 2 considered in the wind tunnel investigation is taken into account. This part of the hall measures 72.9×41.9 m.

Load assumptions

The following loads are assumed. Snow load is once again neglected.

$$q_w = 0.665 \text{ kN/m}^2$$

$$g_{panel} = 0 \text{ (included in ballast quantity)}$$

Considered building geometry:

The building considered here consists of the highlighted section in Figure 4.12, where the module layout is shown in Figure 4.18. The modules are laid out with an angle of 30 degrees with respect to the building walls, facing directly towards south. The height of the building is $z_{ref} = 10$ meters, and the lateral row distance is 2.20 m.

Wind actions

The resulting load areas on the roof considered here are shown in Figure 4.18. The leftmost transient load shown in Figure 4.15 is applied in all load areas of the investigated roof.

Resulting ballast quantities

The ballast quantities necessary to ensure static equilibrium when applying these wind actions are shown in Table 4.2.5, together with the ballast quantities derived using the NVN 7250 wind actions.

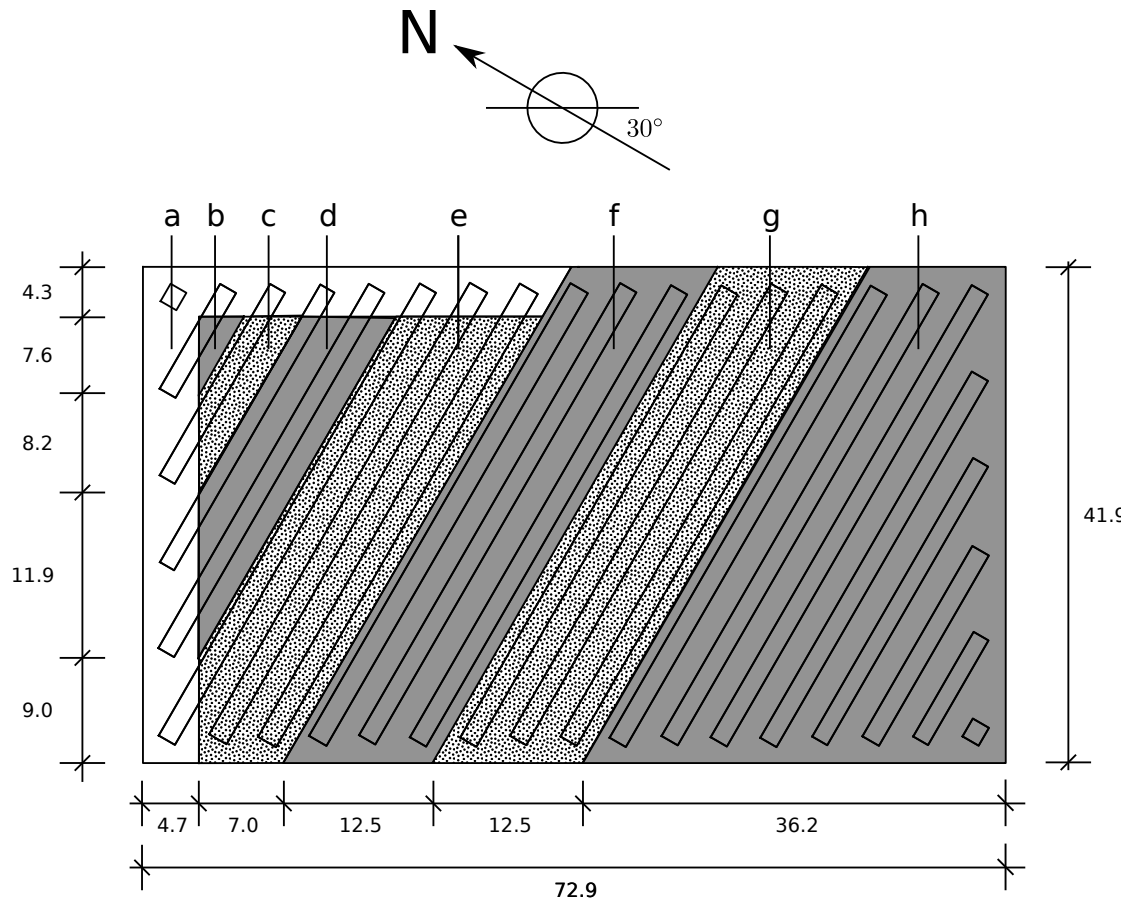


Figure 4.18.: Resulting load areas on the part of the roof considered (Illustration by author)

4.2.5. Adaption of geometry to NVN 7250

The roof is divided into load zones using the method described in section 4.1.2. The same pattern with corner, edge and center zones is formed since the roof is rectangular. Because only one corner of the roof of Hall 2 is regarded for this calculation, the division of the roof is applied to the entire building, and the considered area is cut out, which means that an “L” pattern forms, with corner and edge zones on the north-facing edges of the roof area. Wind actions and ballast quantities are then determined according to the sections 4.1.2 and 4.1.3 respectively. The resulting load zones on the roof are shown in Figure 4.19.

Ballast

The ballast quantities are determined using the method described in section 4.1.3. The amount of ballast is balanced between front and rear support when the derived quantity on the front is larger than the one at the rear, using Equation (4.11). The ballast quantities for selected structures are shown below in Table 4.2.5.

4. Wind actions for varying geometries

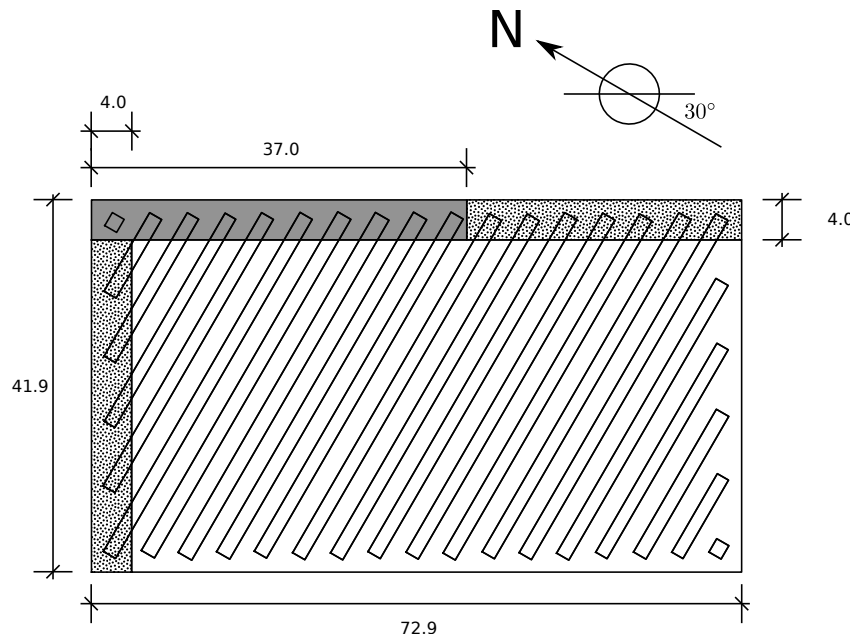


Figure 4.19.: Load zones as derived from NVN 7250.

4.2.6. Comparison

The differences between the ballast quantities derived from the wind actions by Ruscheweyh and Windhövel (2005), and using the NVN 7250 are shown in Figure 4.20, where positive differences indicates an overestimation when using the NVN 7250. The picture was created by creating an evenly spaced mesh over the roof, interpolating the ballast quantities between the coordinates of each support on the roof surface. It seems that the *corner* and *edge* zones from NVN 7250 correspond to the areas with the highest loads according to Ruscheweyh & Windhövel.

Table 4.3.: Ballast quantities for selected structures and the differences between the used approaches. Systems 1.–4. are tagged in Figure 4.20.

Frame	Ruscheweyh & Windhövel	NVN 7250	Difference
Ballast per Support (kN)			
System 1 – Corner zone			
1	0.26	0.92	0.66
2	0.55	2.53	1.98
3	0.26	0.92	0.66
System 2 – Corner/Edges			
1	0.44	1.80	1.36
2	0.42	1.74	1.32
3	0.45	1.83	1.38
4	0.44	1.80	1.36
5	0.44	1.81	1.37
6	0.44	1.79	1.35
7	0.44	1.88	1.44
8	0.44	1.47	1.03
9	0.44	1.26	0.82
10	0.44	2.14	1.70
11	0.45	2.03	1.58
12	0.42	1.96	1.54
13	0.44	2.02	1.58
System 3 – Center, protected			
1	0.29	0.44	0.15
2	0.29	0.44	0.15
3	0.29	0.46	0.17
4	0.29	0.45	0.16
5	0.29	0.45	0.16
6	0.29	0.45	0.16
7	0.29	0.45	0.16
8	0.29	0.45	0.16
9	0.29	0.45	0.16
10	0.29	0.45	0.16
11	0.29	0.46	0.17
12	0.29	0.44	0.15
13	0.29	0.44	0.15
System 4 – Center, protected			
1	0.27	0.22	-0.05
2	0.27	0.56	0.29
3	0.27	0.22	-0.05

4. Wind actions for varying geometries

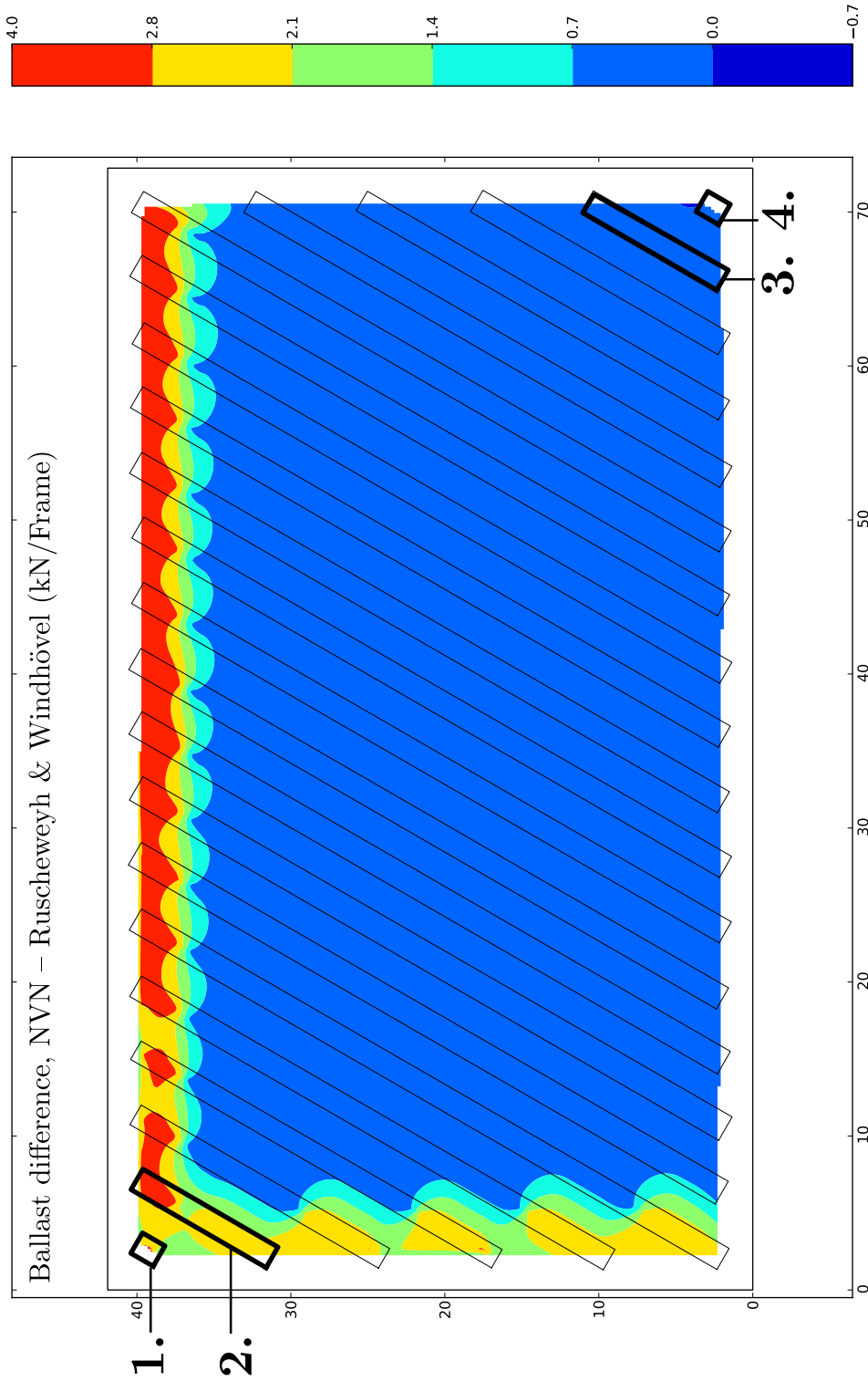


Figure 4.20.: Contour plot of the ballast differences between NVN 7250 and Ruscheweyh and Windhövel (2005). Positive difference indicates that larger ballast quantities were derived using NVN 7250.

The approach to wind loads from the NVN 7250 yields between 1.5 to 5 times as much ballast as the one by Ruscheweyh and Windhövel. A large part of this lies in the different pressure coefficients, where those given in the NVN 7250 (Table 4.1) are circa 5 times as large as those given by Ruscheweyh and Windhövel (Figure 4.14). The necessary ballast for System 3, placed in a protected position in the center of the roof, derived using the NVN 7250, is still larger than the quantities for a *corner zone* structure derived using the pressure coefficients from Ruscheweyh & Windhövel (see Table 4.2.5). It is thus impossible to decide if the zone division suggested by the NVN 7250 is useful in this case, since any division of the roof would have yielded larger uplift forces compared to Ruscheweyh & Windhövel. Finally, it's important to note that the ballast quantities for System 4 are slightly underestimated, probably since the structure is smaller than the transient load area prescribed by Ruscheweyh and Windhövel, turning the transient load into the de-facto load for the entire structure. Structure 4 is however only that small since only a part of the roof was modeled in the wind tunnel.

4.3. Varying roof height

A second, project-specific investigation from Ruscheweyh and Windhövel, considers the wind actions on a building with varying roof height. The varying roof height means that photovoltaic elements normally shadowed by other rows are more exposed to wind actions.

4.3.1. Building and mounting system geometry

Mounting system

Two different module inclinations are considered in the study: 15 and 25 degrees. The module surface has a width of 1 m, and the mounting systems are of the *open* type (see Section 2.1.1). The mounting systems are assumed to have supports each 1.0 m.

Building geometry

The underlying building consists of a single industrial hall measuring 245×125 meters, as shown in Figure 4.21. The nominal roof height of the building is 12 meters, while the height of the hatched parts of the roof amounts to 14 m. The lateral spacing is constantly 1.5 m throughout the entire layout, with some elements omitted due to lanterns and installations.

4.3.2. Wind actions

The wind actions on the modules are described using the same model as in the previous section (see 4.2.2), though the load zone division of the roof and the number of load zones differ. The roof is here divided into 4 areas, with different wind action coefficients shown in figures 4.22–4.23.

Uplift forces are derived for three wind directions: North-West, North and North-East. Wind loads are then assigned to the photovoltaic elements for each wind direction; treated

4. Wind actions for varying geometries

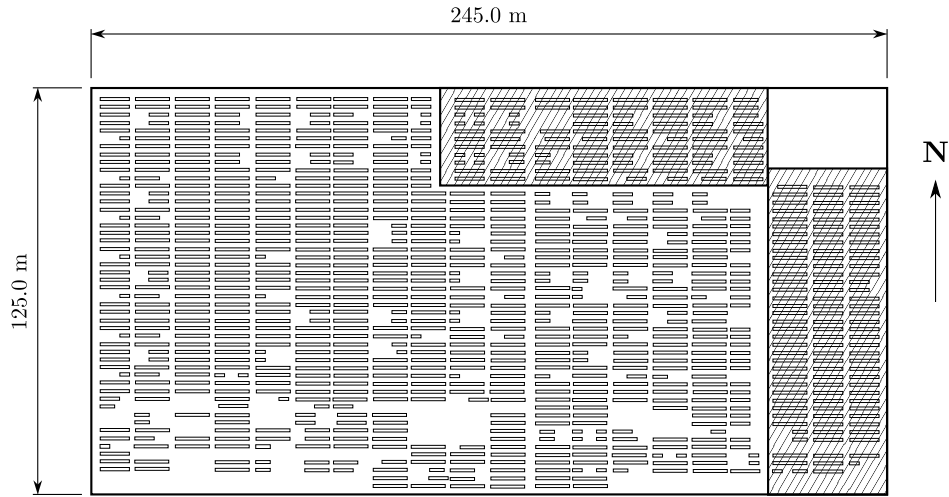


Figure 4.21.: Top view of building roof and module layout (Ruscheweyh and Windhövel, n.d.)

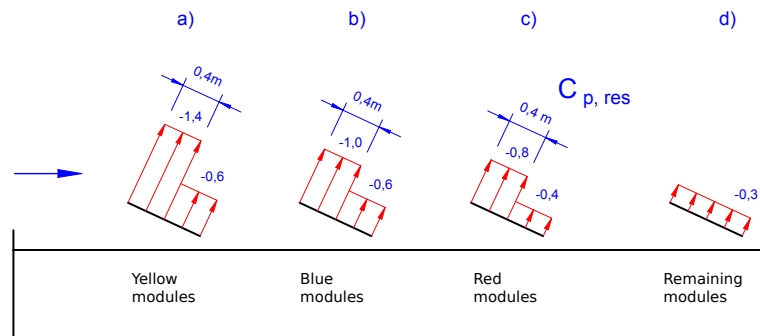


Figure 4.22.: Wind load coefficients for uplift forces, 15 degrees inclination (Ruscheweyh and Windhövel, n.d.)

here, though, is the worst-case scenario for all wind directions. The load zones on the roof are shown in Figure 4.24.

The northern winds are, just like in Section 4.2, assumed to induce uplift forces, while the southern causes downwards pressure. Moreover, a similar force from friction between the air flow and the module surfaces, F_y (compare with Section 4.2.2) is introduced; this time values for the reduction factor ψ_y are provided, ranging between $\psi_y = 0.10$ and $\psi_y = 0.15$. Once again, since the wind friction coefficient is $c_r = 0.02$, these loads are neglected for this comparison.

Straight eastern and western winds (parallel to the module rows) are said to induce no uplift forces; only friction between flow and surfaces. A ψ_y -value of 0.5 is used to determine these forces. It is however clear ($c_{eff} = c_r \cdot \psi_y = 0.01$) that these forces will be smaller than the horizontal forces induced from other blast directions (compare with the blast

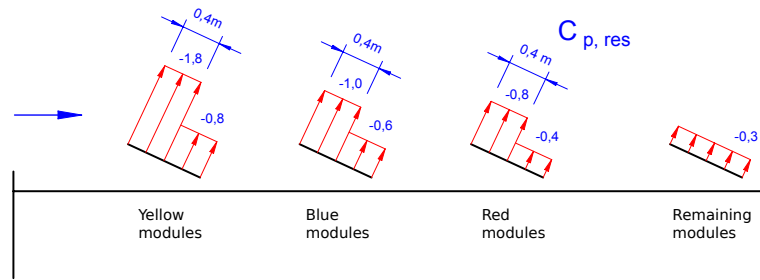


Figure 4.23.: Wind load coefficients for uplift forces, 25 degrees inclination (Ruscheweyh and Windhövel, n.d.)

pressure coefficients from Figure 4.23), and thus this case is not considered for determining the ballast.

Transient loads are used in this approach, just as in Section 4.2.2. Larger transient loads are assumed for the elements in the *yellow* (most exposed) load zone than for remaining elements. The pressure coefficients used for transient loads are shown in Figure 4.25– 4.26.

4.3.3. Ballast

The ballast quantities are determined using the method and assumptions described in Section 4.2.3.

4.3.4. Application of results from case study

Three wind directions (north, northeast and northwest) are, as mentioned above, inducing uplift forces on the solar collectors, and these actions are considered here. The resulting load areas from the different directions are merged to determine the most severe action on each module location (see Figure 4.24).

Load assumptions

The dynamic wind pressure is given in the test report, based on the DIN 1055-4, wind zone 1 and terrain category II, corresponding to the terrain category II of the EN 1991-1-4. The reference height above ground level for the peak velocity pressure is $z = 14$ m.

$$\begin{aligned}
 v_{ref} &= 22.5 \text{ m/s} \\
 q_p(z) &= 0.72 \text{ kN/m}^2 \\
 g_{panel} &= 0 \text{ (Included in ballast)}
 \end{aligned}$$

Wind actions and ballast

The model for wind actions and the process to determine the ballast are described in the sections 4.2.2 and 4.2.3. The length of the mounting systems varies between 3–10.5 m,

4. Wind actions for varying geometries

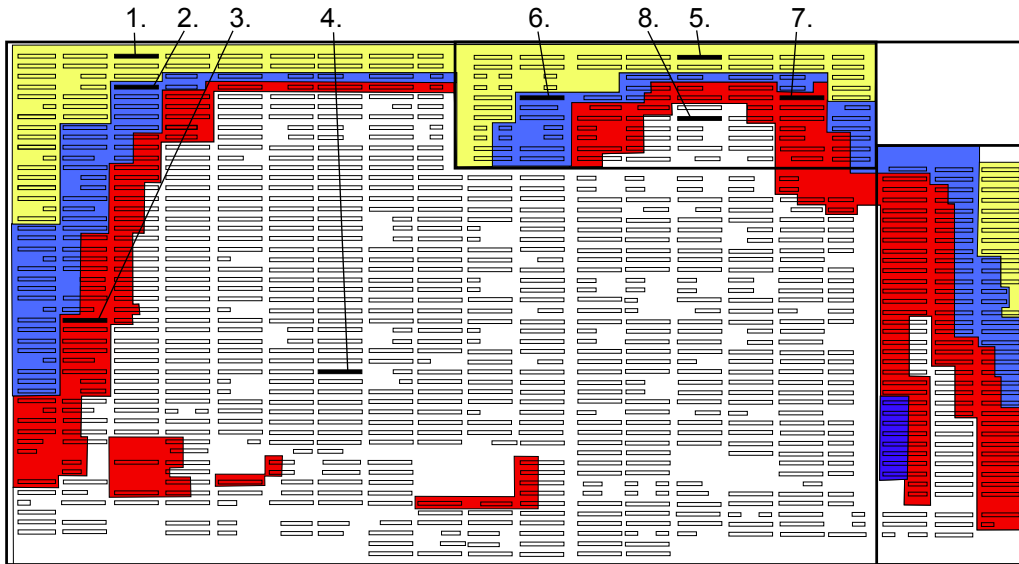


Figure 4.24.: Worst-case wind load zones from northwestern, northeastern and northern winds (Ruscheweyh and Windhövel, n.d.)

which means that the transient loads are applied to a larger share of the structure in comparison to the longer structures in Section 4.2. This, combined with higher wind pressure coefficients than those used in Section 4.2, means that the transient wind loads have larger impact on the ballast quantities for this module layout than in the previous section. Examples of resulting ballast quantities are shown in Table 4.4; since no difference is made between higher and lower roof parts, the positions 5–8 yield the same results as position 1–4.

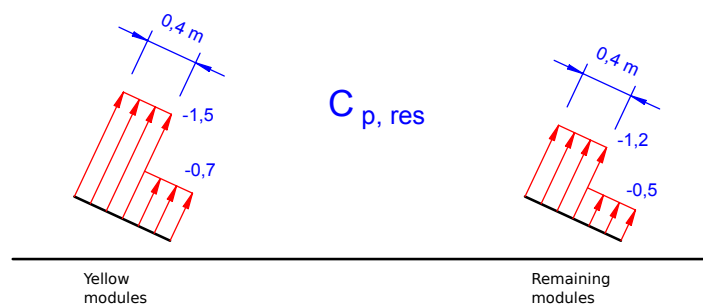


Figure 4.25.: Pressure coefficients for transient loads, inclination 15 degrees (Ruscheweyh and Windhövel, n.d.).

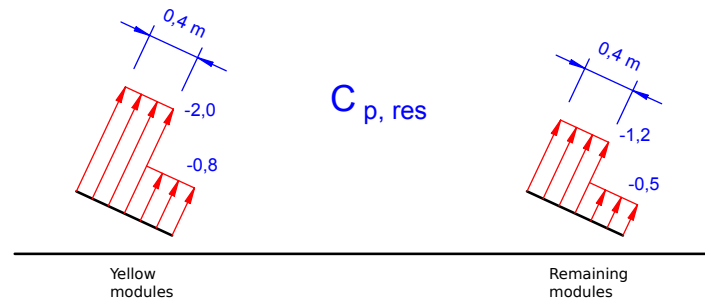


Figure 4.26.: Pressure coefficients for transient loads, inclination 25 degrees (Ruscheweyh and Windhövel, n.d.).

Table 4.4.: Resulting ballast and load/(m² module surface) for different load zones. Structure 1.-4. refers to Figure 4.24.

Structure Inclination	Length (m)	Zone	Ballast kN/support		Ballast kN/m ² module surface	
			15°	25°	15°	25°
1.	10.45	yellow	0.79	1.11	1.66	2.34
2.	10.45	blue	0.59	0.70	1.25	1.47
3.	10.45	red	0.53	0.63	1.12	1.33
4.	10.45	white	0.48	0.57	1.01	1.20

4.3.5. Adaption of roof geometry to NVN 7250

The NVN 7250 provides load zone divisions for roof parts of varying height, specifically for overall height differences and roof lanterns (refer to Appendices A.1 and A.2, respectively), which are applied in the proximity of the height differences. Further, the norm specifies that different peak velocity pressures are to be used on the different roof heights, with the higher pressure to be applied in the additional loading zones just below the the height difference.

Load assumptions

The velocity pressure $q_b(z)$ is derived for the two different roof heights, 12 and 14 m, using the reference velocity given in the Ruscheweyh report. The pressure factors $c_e(z)$ are determined using EN 1991-1-4, chapter 4. In the NVN 7250, the same wind pressure coefficients are used for both 15 degrees and 25 degrees inclination, which is why the calculations are only performed once, using the pressure coefficients shown in Table 4.1

4. Wind actions for varying geometries

from Section 4.1.2.

$$v_b = 22.5 \text{ m/s}$$

$$q_b = \rho \frac{v_b^2}{2} = 0.32 \text{ kN/m}^2$$

$$q_b(12) = c_e(12) \cdot q_b = 2.469 \cdot 0.32 = 0.78 \text{ kN/m}^2$$

$$q_b(14) = c_e(14) \cdot q_b = 2.570 \cdot 0.32 = 0.81 \text{ kN/m}^2$$

Load zones/assignment

To divide the roof into load zones, the standard division from Figure 4.1 is applied to the large roof, using $h = 12 \text{ m}$. The same roof division is then applied to the higher parts of the roof as if they were isolated rectangular roofs. Finally, Appendix A.7 and A.8 (Appendices A.1 and A.2 respectively) are applied to the area below the height differences; though it turns out that these load zones do not intersect with any photovoltaic modules. The load zones on the roof are illustrated in Figure 4.27.

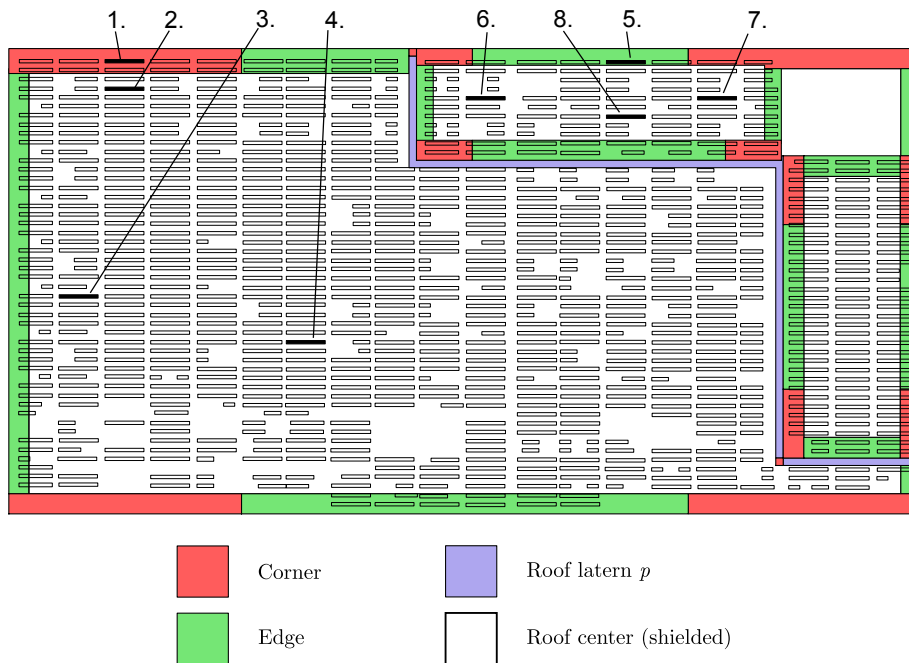


Figure 4.27.: Load zones on the roof as described in the NVN 7250.

Results

The ballast quantities are derived as shown in Section 4.1.3. Table 4.5 shows the ballast quantities derived for the structures referred to in Table 4.4, using the NVN 7250.

Table 4.5.: Ballast quantities derived using the NVN 7250. Structure 1.–8. refers to Figure 4.24.

Structure	Zone	Length	Ballast kN/support	Ballast kN/m ² module
1.	Corner	10.45	1.69	3.55
2.	Center	10.45	0.37	0.79
3.	Center	10.45	0.37	0.79
4.	Center	10.45	0.37	0.79
Structures on higher roof parts				
5.	Edge	10.45	1.56	3.28
6.	Center	10.45	0.39	0.82
7.	Center	10.45	0.39	0.82
8.	Center	10.45	0.39	0.82

4.3.6. Comparison

To compare the ballast quantities on a larger scale (since there are some 900 structures on this roof), the differences between the two approaches are shown as a contour plot (ballast per frame, that is, per two supports). In this diagram, a positive difference means that the NVN 7250 approach has yielded larger uplift forces and more ballast than the wind tunnel investigation. These differences for 15 and 25 degrees inclination are shown in Figure 4.28 and Figure 4.29, respectively, created using the same procedure as with Figure 4.20.

4. Wind actions for varying geometries

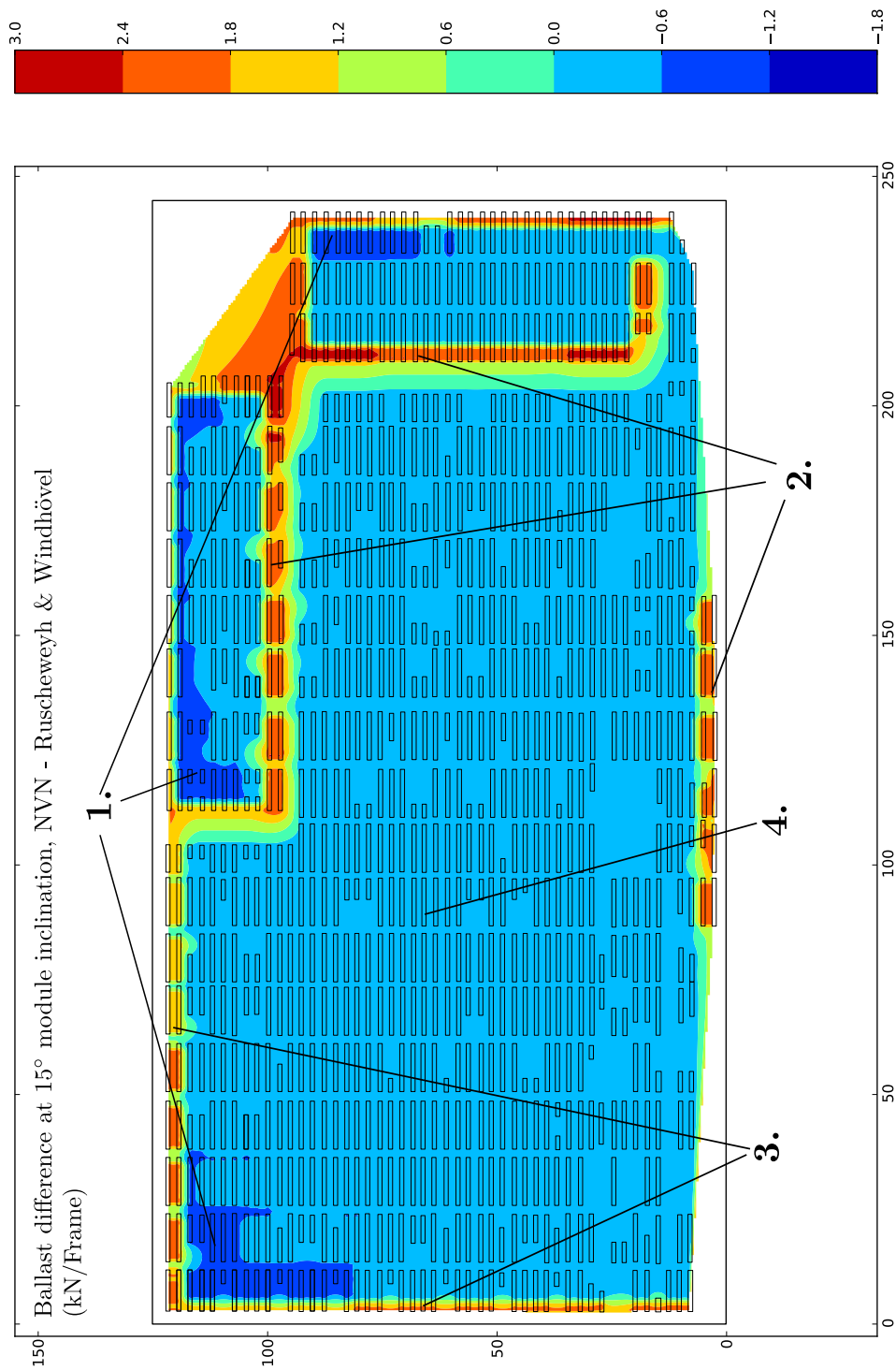


Figure 4.28.: Contour plot of the ballast differences between NVN 7250 and Ruscheweyh and Windhövel (n.d.), module inclination 15 degrees.

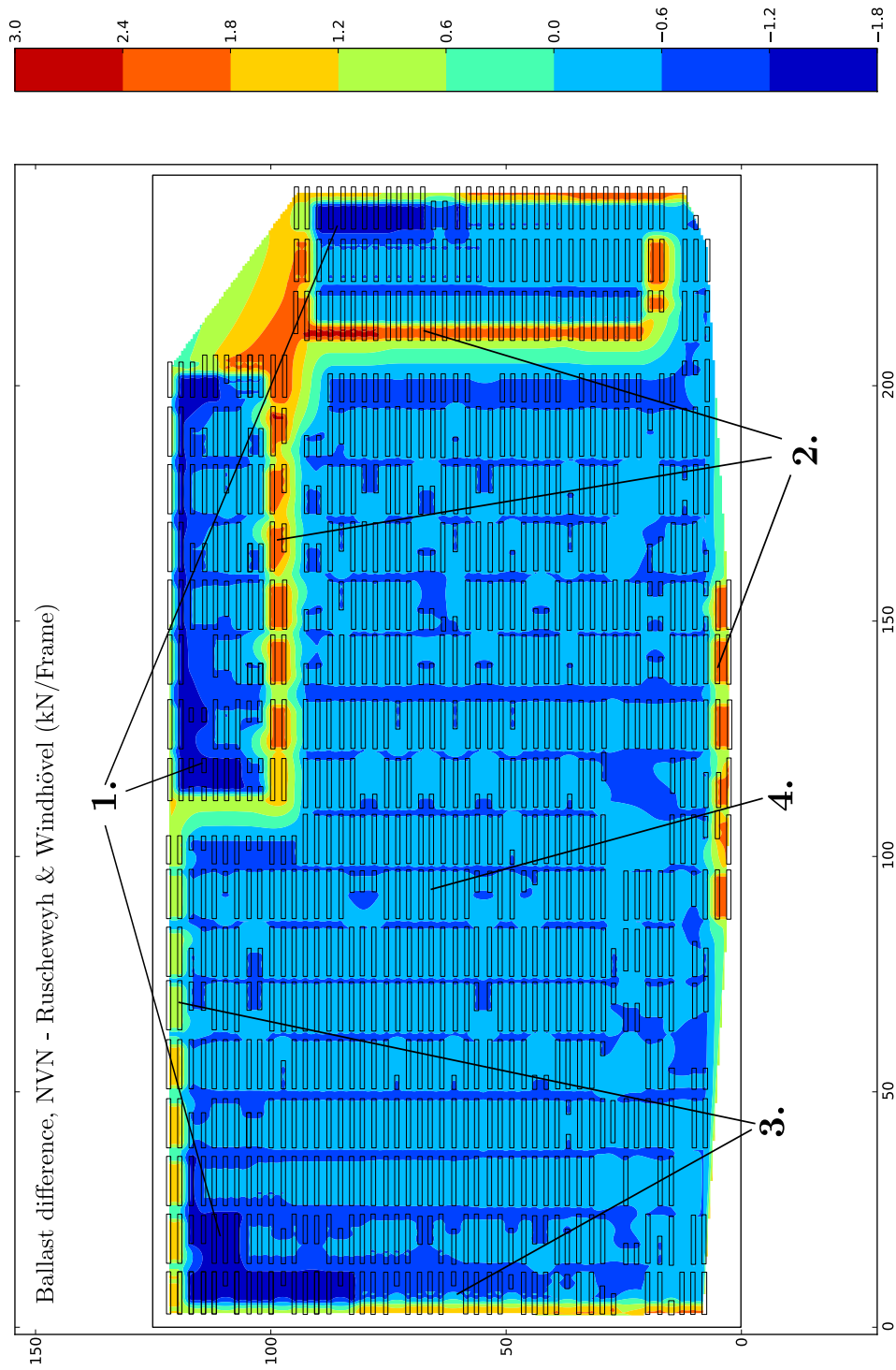


Figure 4.29.: Contour plot of the ballast differences between NVN 7250 and Ruscheweyh and Windhövel (n.d.), module inclination 25 degrees.

4. Wind actions for varying geometries

A few features are highlighted in the figures, the numbers corresponding to the same features:

1. The NVN 7250 misses large exposed areas of the roof stemming from the NW and NE wind directions.
2. The NVN 7250 assigns large uplift forces to roof edges on the lee side of the building, where no large uplift forces occur. This is probably due to the adoption of the load zones from the previous Dutch wind action code, *NEN 6702*.
3. The uplift actions from the NVN 7250 are overestimated along the outer edges of the roof, compared to the wind tunnel results from Ruscheweyh and Windhövel.
4. In general though, the uplift forces and ballast quantities yielded by the approach from the NVN 7250 are underestimated compared to those derived using the results from Ruscheweyh and Windhövel (n.d.). The dark blue stripes in the center (larger underestimations) between mounting systems are residuals from interpolating the ballast differences over the roof area, since it makes no sense that the ballast quantities would increase where no data points (per definition) can exist.

The last point is the most important and needs to be reiterated: It seems to be **not safe** to apply the NVN 7250 for this roof *and* mounting system geometry.

4.4. Standard case, comparison with wind tunnel results

For a roof geometry similar to the one in Section 4.1, a report from wind tunnel tests was provided by Lieb (2010). Only resulting ballast quantities were provided as **kg/module** as dimensioning guidelines for the original customer's products. For comparison with these wind tunnel results, the NVN 7250 is applied to the mounting system geometry presented.

4.4.1. Building and mounting system geometry

Only basic geometry data for the mounting system and the building was provided. The module layout used in the wind tunnel experiment is not known. Instead, ballast quantities necessary to maintain static equilibrium are derived for each roof zone: Corner, edge and center.

Building geometry

The building on which the panels were modelled is a rectangular building, 8×16 m, with a roof height of 10 m. On the building eaves there is a parapet with the height 0.4 m.

Mounting system

The modules have a very gentle inclination of 10 degrees, which still falls into the inclination category "3" (see Section 4.1.1). The photovoltaic panels measure 1.10×1.30 m, and are

4.4. Standard case, comparison with wind tunnel results

mounted horizontally. Unfortunately, no closer description of the mounting system was supplied.

4.4.2. Actions

The dynamic wind pressure used for measurements and derivation of ballast is $q_w = 0.67$ kN/m². Each module is said to have a dead load of 26.5 kg/module, corresponding to a distributed vertical load of $g = 0.185$ kN/m².

4.4.3. Ballast determination

Since the result from the wind tunnel tests are given as ballast tables (with ballast values given in kN/module, according to loading zone), it is not known how this was determined. The process to determine the ballast for comparison is shown in Section 4.1.3.

4.4.4. Application of NVN 7250

Since the module layout wasn't provided, ballast quantities are simply derived for each roof loading zone on a per-module-basis. Because of this, only the dynamic wind pressure and the module measurements have influence on the result. Since the roof parapet is higher than 0.2 m, separate wind loading coefficients are provided in the NVN 7250, see Table 4.6, while the resulting ballast quantities are shown in Table 4.7.

Table 4.6.: Wind load coefficients for different roof areas, for roofs with parapets > 200 mm (Nederlands Normalisatie-instituut, 2007, Table 4).

Roof zone	c_p , upwards	c_p , downwards
c (corner)	-1.5	1.0
r (edge)	-1.2	1.2
p (lantern)	-1.2	1.2
t (center)	-0.6	0.6
t (center, protected)	-0.4	0.4

4.4.5. Comparison

The resulting ballast quantities derived using the NVN 7250 for this geometry are clearly on the conservative side, verging on uneconomical. Since the building geometry used for the wind tunnel investigation is exactly that of the standard geometry described in NVN 7250, the cause of this difference has to be the geometry of the mounting systems investigated by Lieb and those initially investigated for NVN 7250. There is also the possibility that the NVN 7250 simply doesn't sufficiently describe the aerodynamics of the type of mounting systems considered in this section.

4. Wind actions for varying geometries

Table 4.7.: Resulting ballast quantities from Lieb (2010) and NVN 7250.

Roof loading zone	Ballast quantities (kN)	
	Lieb (2010)	NVN 7250
Corner, North	0.716	2.40
Corner, South	0.302	2.40
Edge, North	0.232	1.83
Edge, South	0.247	1.83
Edge, East	0.080	1.83
Edge, West	0.080	1.83
Center	0.000	0.35

4.5. Results and tendencies from the comparisons

In this chapter, the model for the wind actions on roof-mounted photovoltaic panels, used in the NVN 7250 was presented, as well as the method for deriving ballast quantities necessary to maintain static equilibrium of the mounting systems. Further, the results from three aerodynamic case studies were compared with the wind action model and resulting ballast quantities from the NVN 7250, when applied to the specific boundary conditions used in the studies. In case one and three, the ballast quantities could be significantly reduced by applying geometry-specific wind pressure coefficient. On the other hand, the ballast quantities were underestimated over almost the entire roof in the second case.

First of all, it could be concluded that it is not necessary to apply large uplift forces to the southern-facing edges of the building. In case of southern-facing wind, the blast hits the front face of the photovoltaic panels and induces positive (downwards) pressure, with the largest downwards pressure on the outer modules along the south-facing eaves. In case of northern wind, these collector rows are shadowed by the entire building and field of collectors behind them. This makes it unnecessary to apply large uplift forces along the entire building perimeter.

In all cases examined here, the roof geometry remained fairly similar (all rectangular buildings, all of similar height, with dense module layouts), making it improbable that the disparities in resulting ballast quantities are caused by the building geometry. Further, lateral spacing were kept steady in all cases, and no larger roof obstacles were modelled. This leads to the conclusion that the determining factor for the wind loads in the cases treated here are the aerodynamic properties of the mounting structures and photovoltaic panels themselves. That is, the aerodynamic properties of mounting systems brought together in one group in the NVN 7250 seem to vary so widely, that they should not be considered with one group of loading coefficients. The NVN 7250 can therefore not be said to deliver an accurate, nor for all cases safe description of the wind actions on the different mounting systems it attempts to describe.

5. Conclusion

In this study, a structure for mounting photovoltaic panels on flat roofs was described and geometrically parameterized, and a model for static analysis of the structure was developed. Existing approaches to determine the wind loads were presented in the form of general design guidelines (NVN 7250) and the results from 3 wind tunnel experiments, specific to the geometries that were used in the experiments. Using the static model of mounting system, the ballast quantities necessary to maintain static equilibrium under the wind conditions from the design guidelines were derived, and the results from the project-specific approaches compared to those from the general guidelines.

The general wind action guidelines from the NVN 7250 yielded excessive ballast quantities for the boundary conditions from two of the comparisons, while underestimating the ballast quantities on almost the entire module layout compared to the wind actions from the second study. Since all investigated geometries were fairly similar, it was concluded (Section 4.5) that these differences stem from the varying aerodynamic properties of the mounting systems themselves. This is further supported by the variations of the wind loading coefficients between the studies, especially by those from the same institute, using the same model for the wind loads.

Regarding the objective to investigate effects of varying building geometries, no conclusions could be drawn from the material. When the ballast quantities was overestimated by the NVN 7250, they were overestimated to the extent that the most protected modules still experienced more actions than the most exposed modules from the wind tunnel approach. Conversely, wind actions were underestimated over almost the entire area when underestimated by the NVN 7250, making conclusions regarding the different load zones on the roof areas impossible.

5.1. Outlook of creating reusable design guidelines

The existing wind action guidelines for photovoltaic panels, the NVN 7250, seems to define a too coarse classification of mounting systems. A document with accurate descriptions of the available mounting systems would need to cover all the structure types in Section 2.1, and then some; an immense task. Further, the producers of mounting systems would need to classify their own products according to this hypothetical system, perhaps eventually doing wind tunnel experiments anyway just to achieve this. As roof-mounted photovoltaic panels become more common, some researchers believe that available mounting systems will converge into an aerodynamically more optimal design, in a fashion similar to wind power stations. It will then turn into a reasonable task to provide wind loading coefficients for the variations of this hypothetical structure.

5. Conclusion

The current procedure for manufacturers of PV mounting systems has been to determine the aerodynamic properties of the mounting system in a wind tunnel experiments. Some aerodynamics researchers conducting ad-hoc wind tunnel tests claim their results to be product-specific, with loading coefficients reusable for certain variations to the building geometry. Others choose to remain more conservative, providing advice on a project-specific basis. Finally, some researchers have lamented the proprietary nature of these ad-hoc experiments, not furthering the task of creating better design guidelines as the results are kept between the institute and its private customer.

5.2. Critical review of work presented

The initial objective of this study was to investigate the possibilities of assessing the wind actions on photovoltaic panels without conducting repeated wind tunnel experiments. Studies on this area turned out to be few and far between. While it was the original intention to compare more roof geometries and wind load models, and more diverse for that matter, one has to settle for the data actually being available. Perhaps this is a further sign that the area of research hasn't caught on in the academic world, with most of the work being conducted by order of private companies with stakes in the field. Nevertheless, the findings regarding the importance of the mounting system's aerodynamic properties are still significant.

It is further partially due to the proprietary nature of the research conducted in this field that no concrete explanations for the differing results yielded in the experiments being reviewed here are given. Regarding the conclusion of the influence from the mounting system designs, the actual geometries were not disclosed to the author due to non-disclosure-agreements (which, admittedly, have to be obliged when agreed upon in the first place).

Regarding the the work conducted here, the adaptations of the NVN 7250 to the geometries presented in the case studies might seem arbitrary. It would, however, instil a false sense of certainty to adapt these geometries to closely to the known results, while still not knowing how to process unknown roof geometries. Studying the comparisons presented here also show that a further refinement of the adaption of the roof geometry wouldn't have changed the outcome of the comparisons.

5.3. Recommendations for future work at PUK-Werke KG

Since the NVN 7250 proved unusable as a wind action guideline due to the undecided results in the comparisons, this study has still increased the knowledge of PV aerodynamics at PUK-Werke KG. The upcoming tasks at the company would be to settle for a mounting systems' design based on the results of this work, with regard to the general rules of thumb regarding the aerodynamic influence from different features of the mounting system. Once that is settled upon, a wind tunnel experiment should be conducted to derive wind pressure coefficients for safe and economical dimensioning of both mounting systems and fastening.

Bibliography

- Altec Mittig und Manger GmbH (2010). *Altec Alflach*. Accessed on 2010-09-01. URL: <http://www.altec-solartechnik.de/files/11DF8041E9F/ALFLACH.pdf>.
- Blackmore, P. (2004). *BRE Digest 498, Wind loads on roof-based photovoltaic systems*. BRE.
- Boverket (1997). *Boverkets handbok om snö- och vindlast : BSV 97*. Boverket. Karlskrona.
- Bundesministerium für Umwelt, Naturschutz und Reaktorsicherheit (2009). *Erneuerbare Energien in Zahlen*. Niestetal: Bundesministerium für Umwelt, Naturschutz und Reaktorsicherheit.
- (2010). *Erneuerbare-Energien-Gesetz vom 29.03.2000*. Accessed on 2010-10-09. URL: <http://bmu.info/gesetze/verordnungen/doc/2676.php>.
- Bundesverband Solarwirtschaft (2010a). *Solarunternehmen schaffen Arbeitsplätze in Deutschland*. Accessed on 2010-10-08. URL: http://www.solarwirtschaft.de/fileadmin/content_files/solararbpl_0610.jpg.
- (2010b). *Solarzellenproduktion in Deutschland*. Accessed on 2010-10-08. URL: http://www.solarwirtschaft.de/fileadmin/content_files/zellprod_0909.jpg.
- Conergy AG (2010). *Conergy SolarSimplex Fact Sheet*. Accessed on 2010-09-01. URL: http://www.conergy.de/PortalData/1/Resources/produkte/photovoltaik/befestigungssysteme/pdf/IM_Conergy_SolarSimplex_GER_0904.pdf.
- Cook, N.J. (1985). *The designer's guide to wind loading of building structures, Pt. 1*. Cambridge: Butterworths.
- (1990). *The designer's guide to wind loading of building structures, Pt. 2*. Essex: Butterworths.
- Deutsche Institut für Normung (2005). *DIN 1055 Einwirkungen auf Tragwerke - Teil 4: Windlasten*. Deutsche Institut für Normung.
- Erfurth, Reinhard (2001). *Tragkonstruktionen für Solaranlagen – Planungshandlung zur Aufständigung von Solarkollektoren*. Berlin: Solarpraxis Supernova.
- European Committee for Standardization (2002). *Eurocode 0: Basis of structural design*. European Committee for Standardization.
- (2005). *Eurocode 1: Actions on structures, Part 4*. European Committee for Standardization.
- Geurts, Chris P.W. and Carine A. van Bentum (2007). “Wind loads on solar energy roofs”. In: *HERON* 52.3, pp. 201–222.
- Geurts, C.P.W., G.J.P. Ravenhorst, and D.R. Donkervoort (2002). *Windbelasting op zon-collectoren en zonnepanelen op plat-dak opstellingen: deelrapport experimentele bepaling van de ontwerp-windbelasting*. TNO Report 2002-BS-R0061.

Bibliography

- Geurts, C.P.W., C. van Bentum, and P. Blackmore (July 2005). “Wind loads on solar energy systems, mounted on flat roofs”. In: *Paper presented at the 4th European-African Conference on Wind Engineering*. Prague.
- Hilti Deutschland GmbH (2010). *Hilti MSP-AL Flachdachsystem*. Accessed on 2010-09-07. URL: [http://www.hilti.de/fstore/holde/LinkFiles/2_FlatRoofSystem_catalog_W3792_en\[1\]_1.pdf](http://www.hilti.de/fstore/holde/LinkFiles/2_FlatRoofSystem_catalog_W3792_en[1]_1.pdf).
- Isaksson, Tord and Annika Mårtensson (2006). *Byggkonstruktion: tabell- och formelsamling*. Lund: Lunds tekniska högskola, Avdelningen för konstruktionsteknik.
- Janzwig, Bernhard (2010). *Innovationsentwicklung der erneuerbaren Energien*. Accessed on 2010-10-08. URL: http://www.unendlich-viel-energie.de/uploads/media/37_Renews_Spezial_Innovationsentwicklung_durch_EE_Juli10.pdf.
- KNUBIX GmbH (2010). *KNUBIX 100 Fact Sheet*. Accessed on 2010-09-01. URL: http://www.knubix.com/media/downloads/Datenblatt_KNUBIX100.pdf.
- Kösslinger Energy GmbH (2010). *Kösslinger Sunposet Fact Sheet*. Accessed on 2010-09-01. URL: <http://www.koesslinger-energy.de/Userfiles/Broschuere/Broschuere-deutsch.pdf>.
- Lieb, Rolf-Dieter (2009). “Bestimmung der Auflasten eines Solarsystems”. Project-specific case study on behalf of client, made available to the author with project information redacted. Report No. SSB03-1-1. Aachen.
- (Sept. 2010). “Flachdachsystem XYZ”. Project-specific case study on behalf of client, made available to the author with project information redacted. Report Number not given, dated 2010-09-22. Aachen.
- Meskouris, K. and E. Hake (1999). *Statik der Stabtragwerke*. Berlin: Springer.
- Nederlands Normalisatie-instituut (2007). *NVN 7250 Zonne-energiesystemen – Integratie in daken en gevels – Bouwkundige aspecten*. Nederlands Normalisatie-instituut.
- PUK-Werke KG (Jan. 2010). *PUK-Solarline - Montagesystem für Photovoltaik-Anlagen*. Product Catalogue.
- Radu, A. and E. Axinte (1989). “Wind forces on structures supporting solar collectors”. In: *Journal of Wind Engineering & Industrial Aerodynamics* 32.1-2, pp. 93–100.
- Radu, A., E. Axinte, and C. Theohari (1986). “Steady wind pressures on solar collectors on flat-roofed buildings”. In: *Journal of Wind Engineering & Industrial Aerodynamics* 23, pp. 249–258.
- Renusol Solar Mounting Systems (2010a). *Ballastdiagram ConSole 4.1*. Accessed on 2010-09-01. URL: http://www.renusol.com/fileadmin/content/pdf/console/Ballast_ConSole_4.1_31.05.2010.pdf.
- (2010b). *Renusol Consone Fact Sheet*. Accessed on 2010-09-01. URL: http://www.renusol.com/fileadmin/content/pdf/console/Renusol_2S_ConSole_screen.pdf.
- Ruscheweyh, H. and R. Windhövel (2005). “Windlasten an großflächig angeordneten Photovoltaik-elementen”. In: *WtG-Berichte* 9, pp. 155–167.
- (2009). “Windlastminimierung an Photovoltaikanlagen”. In: *WtG-Berichte* 11, pp. 183–187.

- (n.d.). “Windlasten an den Photovoltaik-elementen des Projektes "...””. Project-specific case study on behalf of client, made available to the author with project information redacted.
- Schletter GmbH (2010a). *Schletter CompactGrid*. Accessed on 2010-09-01. URL: http://schletter.de/index.php/de/downloads/doc_download/1825-compactgrid-produktblatt-i400038de.html.
- (2010b). *Schletter CompactVario Fact Sheet*. Accessed on 2010-09-01. URL: http://schletter.de/index.php/de/downloads/doc_download/1826-compactvario-produktblatt-i400037de.html.
- (2010c). *Schletter Solar Montagesysteme — Systemstatik Grundaussführung Flachdach*. Accessed on 2010-09-08. URL: http://www.schletter.de/index.php/de/downloads/doc_download/1686-systemstatik-flachdach-broschuere-i400080de.html.
- Solare Energiesysteme Nord Vertriebsgesellschaft mbH (2010). *SEN SOL-50 Fact Sheet*. Accessed on 2010-09-01. URL: <http://sen.eu/html/img/pool/SEN%20SOL-50%20Flachdachsystem.pdf>.
- Sun-Value GmbH (2010a). *Sun-Value MS-Connect LC3 Fact Sheet*. Accessed on 2010-09-01. URL: http://www.sun-value.com/web/pdf/Prospekt_LC3_2010_03_08.pdf.
- (2010b). *Sun-Value MS-Connect PC2*. Accessed on 2010-09-01. URL: http://www.sun-value.com/web/pdf/Prospekt_PC2_2010_03_08.pdf.
- Sunova AG (2010). *Sunova Befestigung MCG 3.0 Membrane-Connected Glass*. Product Fact Sheet.
- Weller, Bernhard et al. (2009). *Photovoltaik - Technik, Gestaltung, Konstruktion*. Regensburg: Institut für internationale Architektur-Dokumentation GmbH & Co. KG.
- Wood, G.S., R.O. Denoon, and K.C.S. Kwok (2001). “Wind loads on industrial solar panel arrays and supporting roof structure”. In: *Wind & Structures: an international journal* 4.6, pp. 481–494.

A. Excerpts from NVN 7250

A.1. Appendix A.7: Height differences on roofs

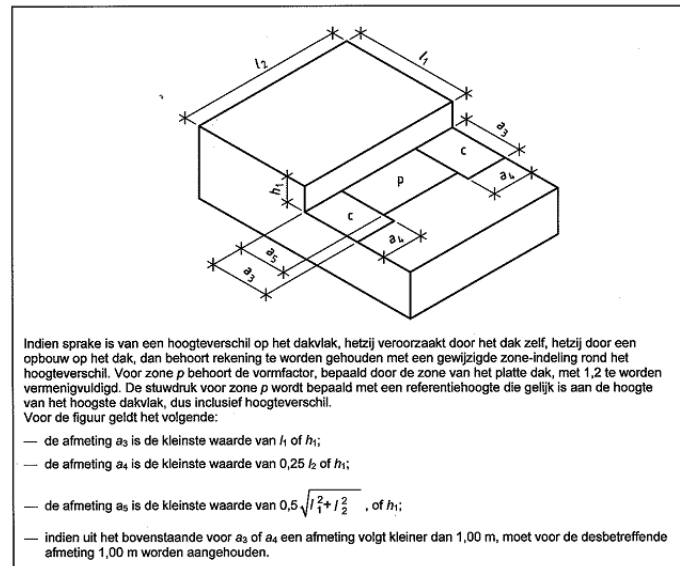


Figure A.1.: Load zones below an overall roof height difference (Nederlands Normalisatie-instituut, 2007, Figure A.7).

Rough translation by the author:

In case of a height difference or a roof lantern, additional loading zones are to be applied in the proximity thereof. The loading coefficient for zone p , determined by its location on the roof (edge, corner, or center) is to be multiplied with a factor 1.2. The dynamic wind pressure applied in zone p is to be determined using the higher of the roof heights as reference height z_{ref} .

In the figure, the following applies:

- The measure a_3 equals the smallest value of l_1 and h_1 .
- The measure a_4 equals the smallest value of $0.25l_1$ and h_1 .
- The measure a_5 equals the smallest value of $\sqrt{l_1^2 + l_2^2}$ and h_1 .
- If any of the measures a_3 and a_4 is smaller than 1.00 m, the measure 1.00 m is to be assumed for the relevant measure.

A.2. Appendix A.8: Roof lanterns and penetrations

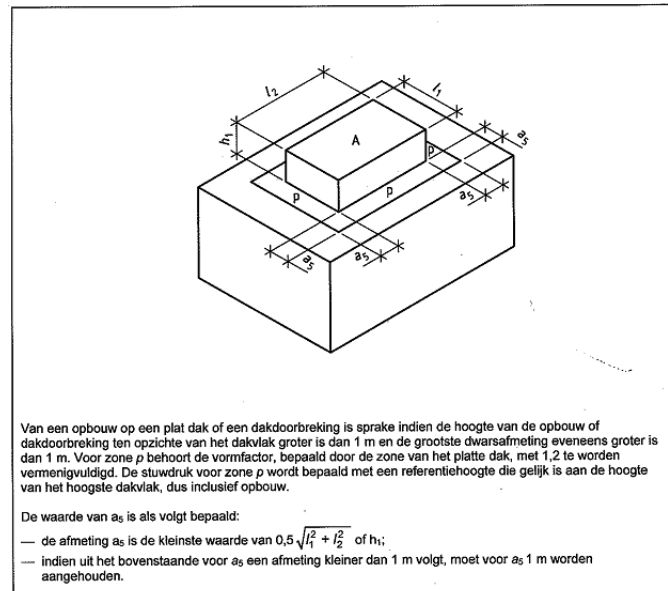


Figure A.2.: Load zones below a roof lantern (Nederlands Normalisatie-instituut, 2007, Figure A.8).

Rough translation by the author:

A roof lantern or roof penetration is defined as a structure higher than 1.0 m relative to the surrounding roofs, with the largest transversal measure also larger than 1 m. In the zone p , the loading coefficient, determined by its location on the roof (corner, edge or center), is to be multiplied with a factor 1.2.

In the figure, the following applies:

- The measure a_5 equals the smallest value of $\sqrt{l_1^2 + l_2^2}$ and h_1 .
- If the measure a_5 is smaller than 1.00 m, the measure 1.00 m is to be assumed for the relevant measure.